C. 2

RESEARCH MEMORANDUM

INVESTIGATION OF THE USE OF AREA SUCTION TO INCREASE THE EFFECTIVENESS OF TRAILING-EDGE FLAPS OF VARIOUS SPANS ON A WING OF 45° SWEEPBACK AND ASPECT RATIO 6

By Roy N. Griffin, Jr., and David H. Hickey

Ames Aeronautical Laboratory
Moffett Field, Calif.

NATIONAL ADVISORY COMMITTEE FOR AERONAUTICS

WASHINGTON

June 22, 1956

NACA RM A56B27

NATIONAL ADVISORY COMMITTEE FOR AERONAUTICS

RESEARCH MEMORANDUM

INVESTIGATION OF THE USE OF AREA SUCTION TO INCREASE THE EFFECTIVENESS OF TRAILING-EDGE FLAPS OF VARIOUS SPANS ON A WING OF 45° SWEEPBACK AND ASPECT RATIO 6

By Roy N. Griffin, Jr., and David H. Hickey

SUMMARY

An investigation was made of a model with a wing of 45° sweepback and aspect ratio 6 to determine the aerodynamic characteristics and suction requirements for boundary-layer control by means of area suction applied to trailing-edge flaps. Included in this study were limited tests of the use of differentially deflected flaps for lateral control. Flap spans extending from 0.12 b/2 to 0.50, 0.66, and 0.83 b/2 were tested at various flap deflections from 46° to 65°. Lateral control tests were made with differential deflections at 46° and 65° on the 0.12 to 0.50 b/2 span flaps with boundary-layer control applied. A limited number of the tests were made with area suction applied to the wing leading edge.

It was found that the area-suction flaps attained the flap lift increment predicted by inviscid-flow theory for the smaller flap deflections and shorter flap spans tested. At the greater values of either deflection or span, area suction did not entirely eliminate flow separation and flap lift increments were somewhat lower than the theoretical values.

The major portion of the lift increment with boundary-layer control was found to be realized when the chordwise extent of the porous opening on the flap was that predicted from tests of a wing of 35° sweepback. In contrast to the results for this other wing, however, the lift was found to increase with an increase in the chordwise extent of porous area up to the largest extent tested. The increased lift was realized in this way only at the cost of relatively high suction quantities.

Measured values of rolling-moment coefficient developed by the differentially deflected flaps with area suction were about 80 percent of

the values predicted by inviscid-flow theory, the difference being due primarily to flow separation on the more highly deflected flap.

INTRODUCTION

A program is being conducted at the Ames Aeronautical Laboratory to determine the effectiveness of area-suction flaps on a series of wings having various plan forms. Reference 1 presented results of tests on a wing of 35° sweepback and aspect ratio 4.78, while reference 2 gave results of tests on a triangular wing of aspect ratio 2. Still unanswered were questions regarding the effectiveness of area-suction flaps of various spans on a wing of higher aspect ratio. It was the purpose of the study herein reported to determine the aerodynamic characteristics and suction requirements for boundary-layer control of area-suction flaps of various spans on a wing of 45° sweepback and aspect ratio 6.

Provision was made to study a range of high flap-deflection angles for each of three flap spans. For the shortest flap span, a study was made of the use of differentially deflected flaps to provide lateral control.

In order to study the flap characteristics beyond the angle of attack for stall of the wing having no leading-edge device, area-suction boundary-layer control was applied to the wing leading edge for some of the tests. Included herein are comparisons of flap lift increment, drag coefficient, and rolling-moment coefficient with those calculated by use of applicable theories. The tests were made in the 40- by 80-foot wind tunnel of the Ames Aeronautical Laboratory.

NOTATION

The forces and moments are referred to the stability axes of the model.

b wing span, ft

C_D drag coefficient, $\frac{\text{drag}}{qS}$

C_{D_i} induced drag coefficient, $\frac{\text{induced drag}}{qS}$

[redacted]

C_L lift coefficient, $\frac{\text{lift}}{qS}$

C_l rolling-moment coefficient, $\frac{\text{rolling moment}}{qSb}$

C_{l_p} rolling moment due to rolling, $\frac{\partial C_l}{\partial(pb/2U)}$, per radian

C_m pitching-moment coefficient, $\frac{\text{pitching moment}}{qS\bar{c}}$

C_n yawing-moment coefficient, $\frac{\text{yawing moment}}{qSb}$

C_{p_f} suction duct pressure coefficient, for flap suction, $\frac{p_d - p}{q}$

$C_{p_{le}}$ suction duct pressure coefficient for leading-edge suction, $\frac{p_d - p}{q}$

C_{Q_f} suction flow coefficient for flap suction, $\frac{Q_f}{US}$

$C_{Q_{le}}$ suction flow coefficient for leading-edge suction, $\frac{Q_{le}}{US}$

c_{l_δ} rate of change of section lift coefficient with flap deflection, per radian

c_{l_α} rate of change of section lift coefficient with angle of attack, per radian

c local wing chord measured parallel to plane of symmetry, ft

[redacted]

$\bar{c}$ wing mean aerodynamic chord, $\frac{\int_0^{b/2} c^2 dy}{\int_0^{b/2} c\, dy}$, ft

c' local chord measured perpendicular to quarter-chord line, ft

c_n section normal-force coefficient, $\frac{\text{section normal force}}{qc}$

d distance along fuselage axis measured from forward end, ft

$\frac{d\alpha}{d\delta}$ lift effectiveness parameter, $\frac{dC_L/d\delta}{dC_L/d\alpha}$

l chordwise extent of porous area on leading edge measured along surface perpendicular to leading edge

P pressure coefficient, $\frac{p_l - p}{q}$

p free-stream static pressure, lb/sq ft

p_l local static pressure, lb/sq ft

p_d suction duct static pressure for leading edge or flap, lb/sq ft

$\frac{pb}{2U}$ wing tip helix angle, radians

Q volume rate of suction flow corrected to standard atmosphere, cu ft/sec

[redacted]

q	free-stream dynamic pressure, lb/sq ft
S	wing area, sq ft
s	chordwise extent of porous opening on flap measured along surface in plane perpendicular to flap hinge line, ft
t	thickness of leading-edge porous material, in.
U	free-stream velocity, ft/sec
w	suction air velocity through porous material, ft/sec
x	distance along airfoil local chord measured parallel to plane of symmetry, ft
y	dimension perpendicular to plane of symmetry, ft
α	angle of attack, deg
β	angle of sideslip, deg
ΔC_D	increment of drag coefficient produced by the deflected flaps at $\alpha = 0^\circ$
ΔC_L	increment of lift coefficient produced by the deflected flaps
Δp	pressure drop through porous material, lb/sq ft
δ_f	flap deflection measured in plane perpendicular to flap hinge line, deg
η_f	dimensionless flap span measured perpendicular to plane of symmetry, fraction of semispan

Subscripts

crit	critical, (minimum value to accomplish boundary-layer control under test conditions)
exp	experiment
f	flap

[redacted]

le	leading edge
max	maximum
min	minimum
th	theory

MODEL AND APPARATUS

The geometry of the model is shown in figure 1, and a photograph of the model mounted for testing in the wind tunnel is shown in figure 2. The wing had 45° sweep of the quarter-chord line of chords parallel to the plane of symmetry, an aspect ratio of 6.0, and taper ratio of 0.292. The airfoil section was constant across the span and had a streamwise thickness ratio of 8.2 percent. The coordinates of the airfoil section are listed in table I. Flush orifices were installed in the left wing of the model for static-pressure-distribution measurements. Table II lists the spanwise and chordwise location of the static-pressure orifices. The dimensions and location of the empennage are shown in figure 1.

Details of the trailing-edge flap and wing leading edge are shown in figure 3. The flap hinge line was located on the lower surface at $0.75c'$ and the flaps were deflected to 46°, 55°, 60°, and 65° measured normal to the flap hinge line. The flap spans which were tested are shown in figure 3. The locations of the outboard ends of the flaps at the trailing edge correspond to 0.50, 0.66, and 0.83 b/2. As shown on the wing plan view in figure 3, the inboard end of the flap hinge line was terminated at a point 2.42 feet from the model center line. For the flap, the exterior surface of the porous area was constructed of metal mesh sheet of 0.008-inch thickness and having 4225 holes per square inch. Beneath the metal mesh sheet was a layer of wool felt of 1/16-inch thickness having the porosity characteristics shown in figure 4. No effort was made to use a material of graded chordwise porosity such as was used in reference 1. The chordwise extent and location of the maximum available porous openings are given in table III.

Details of the porous leading edge of the model are shown in figure 3. The exterior metal mesh sheet was similar to that used on the trailing-edge flap. The porosity characteristics of the wool felt in the leading edge are shown in figure 4. The chordwise thickness distribution of the leading-edge felt was designed by use of the method of reference 3 and is shown in figure 5. The chordwise extent of the porous area at the leading edge also is given in figure 5.

In order to meet the different pressure requirements for leading-edge and flap boundary-layer control, two separate suction systems were

provided. Each of the systems consisted of a centrifugal pump driven by a variable-speed electric motor. In each system, the boundary-layer air removed through the porous area flowed through wing ducts to the pump within the fuselage and was expelled from an exhaust port beneath the fuselage. Each of the exhaust ports was fitted with thermocouples and flow-measuring devices to measure the quantity of air flow required for boundary-layer control.

For the lateral-control study, the same flaps which had been used in the longitudinal study of flap effectiveness were installed to provide differential flap deflections. Hereafter in the report the differentially deflected flaps will be referred to as flaperons.

TESTS AND RESULTS

Longitudinal Tests

Force and pressure-distribution measurements were made for trailing-edge flap deflections of 0°, 46°, 55°, 60°, and 65° and flap spans extending from 0.12 b/2 to 0.50, 0.66, and 0.83 b/2. Tests were made of the foregoing flap configurations without suction on the flap and with varying flap suction flow coefficient, C_{Q_f}, throughout a range of angles of attack from -2° to $+20^\circ$. In those tests in which suction was not applied to the flap, the flap porous area was not sealed as brief tests showed that sealing it with a smooth, nonporous tape produced no change in the lift or drag of the model.

Brief tests were made with each of the flap spans and flap deflections to determine the effect on flap lift increment of varying the chordwise extent of the porous area on the trailing-edge flap with suction applied.

In all of the tests in which suction was not applied to the wing leading edge, the leading-edge porous area was covered with a smooth, nonporous tape.

For most of the longitudinal tests the horizontal tail was removed from the model.

All of the tests were made at a test dynamic pressure of 25 pounds per square foot, giving a Reynolds number of 5.8×10^6 based on the wing mean aerodynamic chord of 6.34 feet.

The following table lists the flap configurations tested and the figures which present data for each configuration.

[redacted]

Flap span, percent semispan	Flap deflection, deg	Figure number
0.12 to 0.50	46	7(a), 8(a), 10(a), 12(a), 13
	55	7(a), 8(a), 10(a), 12(d), 13
	60	7(a), 8(a), 10(a), 12(g), 13, 14
	65	7(a), 8(a), 10(a), 12(i), 13
0.12 to 0.66	46	7(b), 8(b), 10(b), 12(b), 13
	55	6, 7(b), 8(b), 10(b), 12(e), 13
	60	7(b), 8(b), 10(b), 11, 12(h), 13, 14, 15, 16
	65	7(b), 8(b), 9, 10(b), 12(j), 13
0.12 to 0.83	46	7(c), 8(c), 10(c), 12(c), 13
	55	7(c), 8(c), 10(c), 12(f), 13

Lateral Control Tests

In the study of the use of area-suction flaperons for lateral control, the tests covered an angle-of-attack range from 0° to 12° and angles of sideslip from -8° to +8° for one flaperon span (0.12 to 0.50 b/2) and for one differential setting of the flaperons (left flaperon at 65°, right flaperon at 46°). For comparison, tests were made with model having both flaps deflected 55°.

All of the lateral-control tests were made with boundary-layer control applied to the wing leading edge. Most of the lateral-control tests were made by moving the model through a range of sideslip angles while the angle of attack was held constant. The remainder of the tests were made by moving the model through a range of angles of attack while holding the model at a constant angle of sideslip.

Suction flow from each flaperon was adjusted by means of the duct valves to provide that each flaperon would have only sufficient suction applied to maintain attached flow. For comparison with these adjusted flow tests, other tests were made with the duct valves to both flaperons opened to the setting required for the 65° flaperon, thereby providing an excess of suction flow to the 46° flaperon.

It should be noted that the horizontal tail was mounted on the model for the lateral-control tests. This was done to determine the lateral-control effectiveness of the flaperons with the horizontal tail providing its antirolling effect in the unsymmetrical downwash field behind the wing.

[redacted]

The results of the lateral-control tests are presented in figures 17 through 21 inclusive.

The lateral-control tests also were made at Reynolds number of 5.8×10^6.

Flow Coefficients for Boundary-Layer Control

To obtain the data showing the effect of flap suction flow coefficient, the technique used was that of varying the flow coefficient while maintaining constant angle of attack. In tests made with both increasing and decreasing flow coefficient, there was no apparent hysteresis in the variation of flap lift increment with flap suction flow coefficient. A typical variation of the flap lift increment with flow coefficient when area suction is applied to the deflected flaps of the model, is illustrated in the following schematic plot:

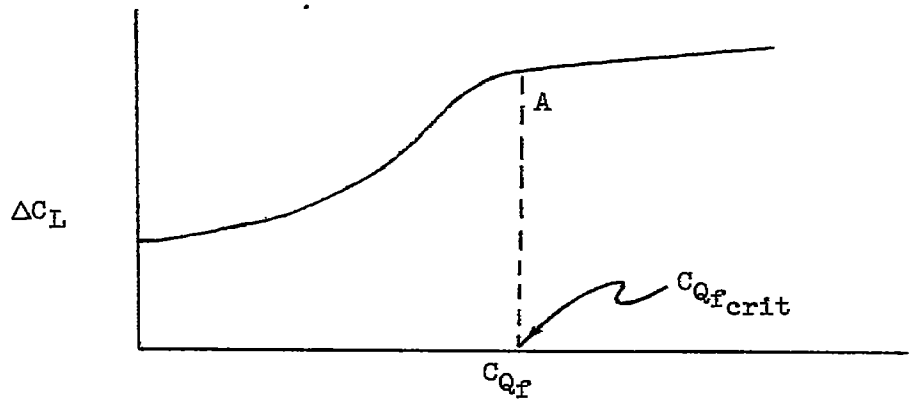

It can be seen that as the lift increment increased with increase in C_{Q_f}, a point was reached (point A) at which the slope decreased and became approximately constant. Further increase in flow coefficient beyond that of point A resulted in relatively smaller gains in flap lift increment. On the basis of tuft observations and static-pressure distributions, it was shown in references 1 and 2 that the greater part of the flow separation on the flap had been eliminated when the flow coefficient at point A was reached. In discussing the aerodynamic characteristics of the model, then, it is necessary to specify the value of C_{Q_f} at which the data are presented. Since point A is believed to be the point of most economical accomplishment of boundary-layer control, most of the data are presented at the flow coefficient associated with that point. The value of C_{Q_f}

at point A is defined as $C_{Q_{f_{crit}}}$. In this report, $C_{Q_{f_{crit}}}$ is conservatively chosen as the nearest data point taken at a C_{Q_f} greater than the minimum value which satisfies the definition. As increments of C_{Q_f} of the order of 0.0001 to 0.0002 were used in testing, the values of $C_{Q_{f_{crit}}}$ presented may be excessive in some cases by approximately those amounts.

Corrections

Tunnel-wall corrections for a straight wing of the same area and span as the model of this test have been applied to the angles of attack and drag coefficients presented herein. This was done since a brief analysis has shown that for wings of the size under consideration the tunnel-wall corrections were approximately the same for straight and swept wings. The following corrections were applied:

$$\Delta\alpha = 0.427\ C_L$$
$$\Delta C_D = 0.0074\ C_L^2$$

No corrections were applied for strut or interference drag. These were not known. All flow coefficients were corrected to standard sea-level conditions. No corrections were made to the data for the jet thrust of the boundary-layer air expelled by the pumps because the thrust was so slight that it was considered negligible.

DISCUSSION

Preliminary Consideration of the Effect of Boundary-Layer Control on Flap Lift Increment

Before consideration is given to the over-all results of applying boundary-layer control to the flaps of the model, it is believed necessary to discuss a basic difference between the present results and those of references 1 and 2 which must be borne in mind when the over-all results are examined.

The initial phase of this study was directed at determining whether the design procedure given in reference 1 and the theory of reference 4 were adequate for predicting the value of critical flow coefficient for the flaps, the external negative pressure and the extent and location of the porous area on the flaps, and the resultant flap lift increments.

Effect of location of rear edge of porous material.- A very important difference was found by this study to exist between the effect of boundary-layer control on the flaps of this wing and that found on the flaps of the wing considered in reference 1. It was found as shown in figure 6 that, with the forward edge of the porous area held fixed at the point of minimum external negative pressure, the lift increment and $C_{Q_{f_{crit}}}$ increased with increase in porous extent up to the maximum chordwise extent tested. The reasons for the difference between this result and those of reference 1, which showed no increase in ΔC_L for s/c' greater than about 0.03, are not known. The results indicated that further increases in lift would have been realized if the porous area could have been extended beyond the maximum value of s/c' physically available, although this would be accompanied by still further increases in $C_{Q_{f_{crit}}}$.

For 55° of flap deflection and various flap spans the following table compares the flap lift increments and values of $C_{Q_{f_{crit}}}$ estimated by the method of reference 1 with values of the same coefficients determined experimentally from tests using the estimated extent $s/c' = 0.030$. In addition, experimental values of ΔC_L and $C_{Q_{f_{crit}}}$ are presented for the maximum available chordwise porous extent, $s/c' = 0.062$.

Flap span	$C_{Q_{f_{crit}}}$			ΔC_L		
	Estimated	Experiment		Estimated	Experiment	
		$s/c' = 0.030$	$s/c' = 0.062$		$s/c' = 0.030$	$s/c' = 0.062$
0.12 to 0.50 b/2	0.00050	0.0006	0.0010	0.755	0.70	0.715
0.12 to 0.66 b/2	.00065	.0007	.0012	.98	.82	.87
0.12 to 0.83 b/2	.00085	.0008	.0016	1.18	.905	.985

These results and those shown in figure 6 are typical of what was found for all flap deflections.

The choice was made to conduct the major part of the investigation with the rear edge of the porous area located as far rearward as possible. All test results discussed subsequently were obtained under this condition. It must be noted that this does not necessarily represent the maximum flap lift increment available nor the maximum value of $\Delta C_L/C_{Q_{f_{crit}}}$.

Effect of location of forward edge of porous material.- It was found that the optimum position of the forward edge of the porous area, as judged

by the greatest lift increment and lowest C_{Q_f} requirement, was at the point of minimum external negative pressure. This result is in accord with the findings of reference 1.

Lift Characteristics of the Model Without Leading-Edge Suction

Effect of suction on lift characteristics.- The lift characteristics of the model without and with boundary-layer control applied to the flaps are presented in figures 7 and 8, respectively.

The values of C_{Q_f} for the data of figure 8 were at or near the critical flow coefficient for each configuration. The chordwise extent of porous area for each flap deflection was that shown in table III. Also shown in figure 8(a) are the lift characteristics for one flap configuration with the horizontal tail on the model.

Lift characteristics at zero angle of attack.- The following table summarizes the lift increment ΔC_L produced by the flaps at $\alpha = 0^\circ$ with $C_{Q_f} = 0$ (from fig. 7) and with $C_{Q_f} = C_{Q_{f_{crit}}}$ (from fig. 8) for the chordwise extents of porous area on the flap shown in table III.

Flap span, b/2	Flap deflection, deg	ΔC_L	
		$C_{Q_f} = 0$	$C_{Q_f} = C_{Q_{f_{crit}}}$
0.12 to 0.50	46	0.475	0.625
	55	.535	.715
	60	.550	.750
	65	.540	.775
0.12 to 0.66	46	.565	.770
	55	.625	.870
	60	.643	.905
	65	.635	.965
0.12 to 0.83	46	.642	.875
	55	.690	.985

Effect of fences on the flap.- It was noted that boundary-layer control at the highest C_{Q_f} available did not prevent flow separation on the

[redacted]

outboard ends of the flaps which extended to 0.66 and 0.83 semispan. Figure 9(a) shows the results of a tuft study of the flow over the 0.12 to 0.66 b/2 span flap deflected 65°. The area of flow separation extended from about 0.50 b/2 to the outboard end of the flap. In an effort to improve the flow over the outer end of the flap and thereby increase the flap lift increment, two small fences were mounted on the flap upper surface at 0.50 and 0.58 b/2. The fences improved the flow over the outboard portion of the flap as indicated by the tuft study shown in figure 9(b) and increased the flap lift increment by about 0.03 at $\alpha = 0°$, as shown in figure 10(b). Since the gain in flap lift increment due to the effect of fences was small, it is not presented elsewhere in the report.

Comparison with theory.- Figure 10 presents a comparison of the flap lift increment, ΔC_L, attained by the model at $\alpha = 0°$ with that predicted by the theory of reference 4 as applied to this plan form. Details of the application of the theory are given in the appendix.

It can be seen in figure 10 that the only flap with suction applied which attains the value of ΔC_L that theory predicts is the 46° flap deflection extending spanwise from 0.12 to 0.50 b/2. It is also to be noted that either an increase in flap deflection for a given flap span or an increase in flap span at constant flap deflection decreased the percentage of theoretical flap lift that was realized. The following table gives the percent of theoretical flap lift increment attained by each of the flap configurations tested without boundary-layer control ($C_{Q_f} = 0$) and with boundary-layer control ($C_{Q_f} = C_{Q_{f_{crit}}}$).

Flap span, b/2	Flap deflection, deg	Percent of theoretical flap lift increment attained	
		$C_{Q_f} = 0$	$C_{Q_f} = C_{Q_{f_{crit}}}$
0.12 to 0.50	46	78	102
	55	71	95
	60	66	90
	65	58	84
0.12 to 0.66	46	71	97
	55	64	89
	60	59	83
	65	53	80
0.12 to 0.83	46	67	92
	55	58	84

[redacted]

The fact that experimental values of ΔC_L for the suction flap were lower than theoretical values at the greater flap deflections results, at least in part, from some degree of flow separation on the flap as has been indicated previously in reference 1 for a flap deflection of 70°.

It is evident from figure 10 that the lift increment produced by the flap without boundary-layer control departs from theory at some flap deflection smaller than 46° for all of the flap spans tested. It should be noted, however, that the theoretical values of ΔC_L presented in figure 10 were obtained by the use of the theoretical two-dimensional value of $d\alpha/d\delta$ for this flap-chord ratio. Brief calculations, made for the 0.12 to 0.50 b/2 span flap only, show that if, instead of the theoretical value of $d\alpha/d\delta$, one uses an experimental two-dimensional value obtained in the range of $\delta_f = 0°$ to 20°, the flap lift increment attained by the model with $\delta_f = 46°$ and without suction is equal to the theoretical value. Thus it appears that the lift increment produced by the flap without boundary-layer control is somewhat higher than might be expected. The fact that a plain flap on a sweptback wing is as effective as it is in producing lift appears to be related to three-dimensional boundary-layer phenomena. The spanwise flow within the boundary layer apparently is, in effect, a natural boundary-layer control for the inboard sections of the flap.

Lift characteristics at higher angles of attack.- In figures 7 and 8, it can be noted that the maximum lift coefficient attained with or without suction for a given flap span is approximately the same for all flap deflections tested greater than $\delta_f = 0°$. This results from the fact that the maximum lift is limited by flow separation from the wing leading edge as indicated by the static-pressure distributions presented in figure 11. The flap was deflected 60° and extended from 0.14 to 0.66 b/2.

Drag Characteristics of the Model Without Leading-Edge Suction

Effect of suction on drag.- One of the primary points of interest is the effect of boundary-layer control on the drag of the model with flaps deflected. Comparison of the drag coefficients at $\alpha = 0°$ for the same configurations in figures 7 and 8, shows that for the longer flap spans, the drag with suction applied is less than the drag without suction. This result would indicate that when boundary-layer control was applied, the reduction in drag due to flow separation was of greater magnitude than the increase in induced drag due to higher lift.

Comparison of the drag coefficients of the various flap spans with suction applied (fig. 8), shows that at a given lift coefficient in the linear lift range, the drag coefficient is smaller for the longer flap

spans than for the shorter. This follows from the fact that the induced drag is less since elliptic spanwise loading is more closely approached with the longer flap spans.

Comparison with theoretical drag.- Because of the effects that area suction has on the profile and induced drag, it may be of interest (in performance calculations, for example) to determine to what degree of accuracy the drag of the model with flaps deflected can be estimated from theoretical drag considerations. For this purpose, a comparison is made in figure 12 of the experimental lift-drag polars of the model with and without suction on the flaps and the theoretical polars for the same configurations as calculated by the method of reference 5. The theoretical polars were calculated at the same angles of attack at which the experimental data were obtained. Details of the application of the theory are given in the appendix. In figure 12 it is seen that good agreement was obtained between theory and the area-suction flap data for the model with the smaller flap deflections and shorter flap spans. At the greater flap deflections and longer flap spans, there is poorer agreement between theory and experiment. In those cases where the agreement is not good, the curves for theory and experiment with suction appear to lie in reasonable proximity. This should not be taken to mean that agreement in drag coefficient is obtained if theory and experiment are compared at equal lift coefficients. Such a comparison is not valid since the differences in angle of attack involve differences in shape of the span load distributions and consequently different induced drag. The proximity of the experimental and theoretical curves at the greater flap deflections and longer flap spans results, in part, from profile drag due to flow separation which was not eliminated by suction and must be considered fortuitous.

Also shown for purposes of comparison in figure 12(d) are unpublished data for a model having a double-slotted flap. The wing had 45° of sweepback, an aspect ratio of 6, and a taper ratio of 0.5. The flap span extended from 0.18 b/2 to 0.58 b/2, the flap deflection was 55°, and the flap-chord ratio c_f/c' was 0.25 for the main flap. These data also were obtained in the Ames 40- by 80-foot wind tunnel. The data are presented at the same angles of attack as the area-suction flap data and the theory. In order to compare the polars of the area-suction flap and double-slotted flap directly, the model with the double-slotted flaps was assigned the same flaps-up minimum drag as the model with the area-suction flaps. At a given angle of attack, the double-slotted flap gave somewhat higher lift than the plain flap without suction, but not as high lift as the suction flap. The drag of the double-slotted flap at a given angle of attack was higher than that of either the plain flap or the area-suction flap.

The extent to which area suction causes the drag coefficient of the model to approach the value predicted by inviscid flow theory can be seen in figure 13. The high values of the parameter $(\Delta C_D/\Delta C_L^2)_{exp}/(\Delta C_D/\Delta C_L^2)_{th}$ for the flaps without suction indicate high profile drag for all of the

[redacted]

flap configurations. Furthermore, the increasing values of the parameter with greater flap deflections for the case without suction show the effects of increased flow separation drag. With area suction applied to the flaps, the values of the parameter become essentially 1.0, indicating that the drag with boundary-layer control is largely induced drag.

Pitching-Moment Characteristics Without Leading-Edge Suction

The effect of boundary-layer control on the pitching-moment coefficient can be seen in a comparison of figures 7 and 8. Applying suction to the deflected flaps increased the magnitude of the negative pitching-moment coefficient.

Incremental values of C_m/C_L for the area-suction flaps are found to be of slightly greater absolute magnitude than the values for the same flap without suction, all values being calculated at constant angle of attack from the data presented in figures 7 and 8. This result is different from the results of the test of reference 1 which showed a reduction in magnitude of incremental value of C_m/C_L when suction was applied to the flap.

In figure 8(a) are shown the longitudinal characteristics of the model with the 60° flap extending from 0.12 to 0.50 b/2 with suction applied and with the horizontal tail on. It is seen that after the unstable break in the pitching-moment curve occurring at 8.5°, the horizontal tail provided stable pitching moments up to the highest angle of attack tested. At an angle of attack of 0.4° the trim lift coefficient was 0.715 as compared to the lift coefficient of 0.77 obtained with the horizontal tail removed. Although data were not obtained for the 0.12 to 0.66 b/2 span flap, calculations show that for the same angle of attack, the trim lift coefficient for the 60° deflection with suction would be 0.84 as compared to 0.93 obtained with the horizontal tail off.

Suction Requirements for Boundary-Layer Control on the Flap

Suction flow requirements.- The suction flow coefficients, $C_{Q_{f_{crit}}}$, required for boundary-layer control on the flap configurations tested are given in table III. The values presented were obtained by variation of the suction flow coefficient at zero angle of attack. The magnitude of the peak negative pressures on the flap became smaller with increasing angle of attack (fig. 11), presumably as a result of the thickening of the upper surface boundary layer. In consequence, the flap duct pressures

[redacted]

required to give $C_{Q_{f_{crit}}}$ at the higher angles of attack were correspondingly reduced, although the values of $C_{Q_{f_{crit}}}$ at higher angles of attack were approximately the same as those at $\alpha = 0$.

The flow coefficient required for boundary-layer control is a function of the porosity characteristics of the porous material and the external static-pressure distribution over the porous surface. The porous material tested had constant permeability chordwise and spanwise, therefore all values of $C_{Q_{f_{crit}}}$ presented are probably considerably higher than would be required for a porous material having its permeability varied to give more uniform suction velocity through the porous material. In the tests of reference 1, it was found that $C_{Q_{f_{crit}}}$ reductions as great as 55 percent could be achieved by this means.

Suction pressure requirements.- The suction pressure coefficients required for boundary-layer control on the various flap configurations are shown in table III. The suction pressure coefficient associated with the flow coefficient, $C_{Q_{f_{crit}}}$, will be designated $C_{p_{f_{crit}}}$. The most important factor affecting $C_{p_{f_{crit}}}$ is the magnitude of the minimum external static pressure on the flap, a secondary factor being the permeability characteristics of the porous material through which the boundary-layer air is removed. The importance of the minimum external static pressure may be seen by a comparison of the minimum external static-pressure coefficient, P_{min}, and $C_{p_{f_{crit}}}$ for the 60° flap extending from 0.12 to 0.66 b/2. Table III shows a value of -4.18 for $C_{p_{f_{crit}}}$ while P_{min} had a value of -4.10 as shown at $\alpha = 0.4°$ in figure 11. As the external static-pressure orifices were located about 1.0-percent chord apart on the flap arc, it is possible that the actual value of P_{min} may not have been measured due to its location between orifices, but it is believed that the figure -4.10 is reasonably close to P_{min}. Good agreement was obtained between experimental values of P_{min} on the flap upper surface and those estimated by the method of reference 1 as shown in the following table:

δ_f, deg	Estimated P_{min}	Experimental P_{min}
46	-3.1	-3.1
55	-3.8	-3.8
60	-4.2	-4.1
65	-4.6	-4.5

[redacted]

Aerodynamic Characteristics of the Model With Boundary-Layer Control Applied to the Flaps and the Wing Leading Edge

In order to study the effects of boundary-layer control on the flap at angles of attack beyond the stall of the wing with the leading edge sealed, area suction was applied to the wing leading edge. Data are presented only for the case of the 60° flap deflection extending from 0.12 to 0.50 and 0.66 b/2 as these are sufficient to show the flap effectiveness at higher angles of attack. Figure 14 shows the lift, drag, and pitching-moment characteristics for these two flap spans with and without area suction at the wing leading edge and on the flap. These data represent the characteristics at or slightly above $C_{Q_{f_{crit}}}$ for the flap suction. It is evident from examination of figure 14 that the effectiveness of an area-suction flap is maintained to higher angles of attack if a leading-edge device is used to delay leading-edge flow separation.

The suction requirements for the flap and leading-edge boundary-layer control are shown in table IV. The $C_{Q_{le}}$ and $C_{p_{le}}$ for the leading-edge suction were maintained at values above those required to prevent leading-edge flow separation at each angle of attack for each configuration. Because it was felt that $C_{Q_{le}}$ and $C_{p_{le}}$ were considered of secondary interest, no attempt was made to determine the minimum values to prevent separation. The $C_{Q_{f_{crit}}}$ and $C_{p_{f_{crit}}}$ required for the flap were approximately the same values as were required for the wing without leading-edge suction.

Figure 15 shows the wing static-pressure distributions for the 60° flap deflection extending from 0.12 to 0.66 b/2 with area suction at the leading edge. These data were taken from the tests for which the force data are presented in figure 14. As the angle of attack was increased above 0° the magnitude of the minimum pressure peak on the flap decreased although no flow separation had occurred on the forward part of the wing. A similar phenomenon was previously pointed out for the case of the wing without area suction at the leading edge.

When area suction was applied to the flaps with the wing leading edge sealed, the maximum value of c_n of each section shown in figure 16 was limited by flow separation from the wing leading edge. Maximum lift of the model occurred when the outer section of the flap (0.585 b/2) reached its maximum c_n at about 8.5° angle of attack.

When area suction was applied to the wing leading edge as well as to the flaps, the section normal-force coefficients continued to increase up

to the highest angle of attack tested, but with decreasing slope. The data presented in figure 16 were obtained from the data presented in figures 11 and 15.

Lateral-Control Study

Shown in figure 17 are the rolling-moment data for the model with the 55° flap deflection with C_{Q_f} held constant at a value of 0.0019 which is somewhat above $C_{Q_{f_{crit}}}$. The leading-edge flow coefficient at each angle of attack was that required to prevent flow separation from the leading edge.

Figure 18 presents the rolling-moment data for the model with the left flaperon deflected 65° and the right flaperon deflected 46°. The flaperon suction duct pressures were adjusted so that the value of each flaperon flow coefficient was at or slightly above $C_{Q_{f_{crit}}}$ for its deflection. The data of figure 18 show that at $\beta = 0°$, a rolling-moment coefficient of about 0.016 was developed at $\alpha = 0.3°$ due to the differential flaperon deflection. This compares with a value of 0.022 (for the wing alone) as predicted by the method of reference 6. An outline of the application of reference 6 to this model is given in the appendix of this report. The effect of the empennage in the asymmetric downwash field is that of reducing the rolling moment of the model. A computation briefly outlined in the appendix was made to determine the magnitude of the effect of the horizontal tail. The tail contribution was found to be -0.002 rolling-moment coefficient. The effect of the vertical tail is believed to be somewhat smaller than that of the horizontal tail and therefore was not estimated. Comparison of the experimental value of 0.016 to the theoretical of 0.020 with the tail on shows that 80 percent of theoretical rolling-moment coefficient was attained. The failure of the model to attain the expected rolling-moment coefficient can be largely attributed to the fact that the flaperon deflected to 65° does not attain the theoretical lift.

A brief test was made in which the suction-flow coefficient was not adjusted to the requirements of each flaperon. Instead, the suction flow from both wings was adjusted to the requirements of the 65° deflection, with the result that the flaperon deflected 46° had considerable excess flow and consequently somewhat increased lift. This arrangement resulted in a reduction of 25 percent in the rolling-moment coefficient developed by the model (0.012 at $\alpha = 0.3°$ as compared to the 0.016 previously attained with adjusted suction), and emphasized the possible need for adjusting the flow to the flaperon requirements.

[redacted]

Brief calculations, based upon the experimental rolling-moment coefficient of 0.016 and a value of $C_{l_p} = -0.342$ obtained from reference 6, for this plan form indicate that the value of wing-tip helix angle, pb/2U, for the flaperon configuration tested would be about 0.046. Although this value of pb/2U is lower than the minimum of 0.07 specified in reference 7 for satisfactory flying qualities, it should be noted that the rolling-moment coefficient of 0.016 was obtained with relatively small differential deflections of flaperons extending from 0.12 to 0.50 b/2. An increase in flaperon span, possibly combined with somewhat greater differential deflections, would probably result in adequate roll control.

One factor which may affect the utility of area-suction flaperons at high deflections for roll control is the adverse yawing moment developed. Figure 19 presents the yawing-moment coefficient variation with sideslip angle for the same test conditions for which the rolling-moment data are presented in figure 18. At zero sideslip, the adverse yawing-moment coefficient was about -0.003 in the low angle-of-attack range and zero at the highest angle of attack tested.

Figure 20 shows the rolling-moment coefficient developed by the model with the 46° and 65° flaperon deflections with boundary-layer control as the lift coefficient was increased while the sideslip angle was held constant. The negative slope of the curve for $\beta = 0^\circ$ indicates that the effectiveness of the 65° flaperon was decreasing more rapidly than that of the 46° flaperon as the angle of attack was increased. Comparison of the data in figures 18 and 20 shows only negligible differences in rolling-moment coefficient for corresponding angles of attack and sideslip, indicating that the areas of the wing on which flow separation existed were probably similar in both cases.

Figure 21 presents the yawing-moment coefficient variation with lift coefficient from the same test for which rolling-moment data were presented in figure 20. At $\beta = 0^\circ$ an adverse yawing-moment coefficient of about 0.002 is to be noted in the linear lift range.

CONCLUDING REMARKS

The results of the wind-tunnel investigation of area-suction flaps of various deflections and spans and of flaperons on a wing of 45° sweepback and of aspect ratio 6 indicate that the lift coefficient developed by the suction flaps continued to increase with increasing flap deflection up to a deflection of 65°, the highest value tested, but at a reduced rate at the higher deflections due to the inability of the suction to eliminate the flow separation completely.

[redacted]

It was found that the values of lift and drag coefficients due to flaps on which negligible flow separation existed could be predicted with good accuracy by use of the theories of references 4 and 5. This was evidenced by the agreement at the smaller flap deflections and shorter flap spans. It is believed that greater chordwise extents of porous area than those tested would give closer agreement to theoretical flap lift at the higher flap deflections since, for those deflections, the flap lift increment at $C_{Q_{f_{crit}}}$ continued to increase with increased chordwise extent of porous area. Such an increase in chordwise extent of porous area probably would result in higher critical flow coefficients since it was found that increasing the chordwise extent by about a factor of 2 in order to obtain higher lift approximately doubled the critical flow coefficient.

Experimental flap suction flow coefficients were in good agreement with those estimated by the method of reference 1 for the same chordwise extent of porous area used in the test of reference 1.

Good agreement was found between the pressure coefficients required for flap suction and those estimated by the method of reference 1.

The measured values of rolling-moment coefficient developed by the area-suction flaperons tested were somewhat lower than the calculated values. This result is believed to be due to some degree of air-flow separation on the more highly deflected flaperon as well as to the anti-rolling effect of the empennage in the wake of the wing. The use of area-suction flaperons appears to be feasible as a means of producing roll control for airplanes having sweptback wings.

Ames Aeronautical Laboratory
National Advisory Committee for Aeronautics
Moffett Field, Calif., Feb. 27, 1956

[redacted]

APPENDIX

BRIEF DISCUSSION OF THE APPLICATION OF THE THEORIES OF REFERENCES 4, 5, AND 6

For the purpose of enabling the reader to follow the application of the theories of references 4, 5, and 6 in estimating the lift and induced-drag coefficients due to the deflected flaps and the rolling-moment coefficient due to flaperons, pertinent information will be given here concerning the assumptions made, necessary additional information about the model geometry, and, in brief, the procedure followed. No detailed discussion of the application of the theories is needed here, as it is given adequately in the above references.

Calculation of Theoretical Flap Lift Increment

Model geometry and assumptions.- In order to apply the theory of reference 4 to calculate the lift due to deflected flaps, it is desirable to express the model dimensions in terms compatible with the equations of that report. The model of this test had a flap-chord to wing-chord ratio, c_f/c, of 0.214 in planes parallel to the plane of symmetry and the sweepback of the flap hinge line was 39.17°. The additional model geometrical characteristics needed to calculate ΔC_L due to the deflected flaps are shown in figure 1 of this report. The calculations of flap lift are for the wing alone, no fuselage effects being considered.

Procedure.- The theoretical value of the parameter $d\alpha/d\delta$ of 0.565 obtained from figure 3 of reference 4 was used in the calculations. This was done because experience has shown that calculations, in which experimental values of $d\alpha/d\delta$ taken in the range of small flap deflections were used, predict lower values of ΔC_L than are obtained experimentally on sweptback wings on which little or no flow separation is present. In application of the theory of reference 4 to this model, the inboard flap case was used, and it is to be noted that the model had constant fraction of wing-chord flaps. For simplicity, both β, the compressibility parameter, and κ_{av}, the lift-curve slope parameter, were assumed equal to 1.0. Then by following the steps outlined in reference 4 the theoretical flap effectiveness was obtained for the experimental flap deflections.

Calculation of Theoretical Lift-Drag Polars

Calculation of lift coefficient.- The lift-coefficient increments due to flap deflection and angle-of-attack change are directly additive as indicated in reference 4. Since the flap lift increments had been calculated for each of the various flap configurations at zero angle of attack, it was necessary only to determine the increase in lift coefficient due to change in angle of attack. This was done by the method of reference 5. For purposes of comparison with experimental data, the theoretical values of lift coefficient were calculated from C_{l_α} (obtained from ref. 5) at the same angles of attack at which experimental data were taken.

Calculation of drag coefficient.- The theoretical drag coefficient of the model can be expressed as

$$C_D = C_{D_{min}} + C_{D_i}$$

where $C_{D_{min}}$ is the minimum drag coefficient of the model with flaps undeflected and C_{D_i} is the induced drag coefficient resulting from the total loading due to the flap deflection and angle of attack. An experimental value for $C_{D_{min}}$ of 0.0351 had been obtained at $\alpha = 0^\circ$ with the flaps undeflected, so it was necessary only to compute C_{D_i} for the model with the various flap configurations at the angles of attack for which C_L had been calculated. The induced drag coefficients were computed by the method of reference 5, and total drag coefficients were obtained by addition of $C_{D_{min}}$ to the theoretical values of C_{D_i}.

Estimation of Rolling-Moment Coefficient Developed by the Flaperons

Calculation of rolling-moment coefficient.- The application of the method of reference 6 to calculate the rolling-moment coefficient developed by the flaperons is somewhat analogous to that previously used in determining the theoretical flap lift increment. Span loadings were calculated for full wing-chord ailerons. Once again β and κ_{av} were assumed equal to 1.0. Reference 6 was then used to obtain a value of $C_{l_{\delta_t}}$, the aileron effectiveness parameter for constant fraction of wing-chord ailerons. Appropriate values of flaperon deflection measured parallel to the plane of symmetry were then substituted to obtain the calculated values of rolling-moment coefficient due to flaperon deflection for the wing alone.

[redacted]

Since the effect of the empennage in the asymmetric downwash field behind the wing was that of reducing the rolling moment produced by the flaperons, a correction accounting for the effect of the horizontal tail was applied to the calculated rolling-moment coefficient for the wing alone. The effect of the vertical tail was believed to be smaller than that of the horizontal tail; therefore it was neglected.

The horizontal-tail contribution to the rolling moment was computed after first calculating by the method of reference 6 the antisymmetric loading on the wing due to the differential flap deflection. The downwash, w/V, across the horizontal tail was then computed from the equation

$$\left(\frac{w}{V}\right)_{\frac{\xi}{\beta},\eta_\nu} = \sum_{n=1}^{3} p_{\nu n} G_n$$

where ξ/β and η_ν are dimensionless longitudinal and lateral coordinates and $p_{\nu n}$ is a coefficient depending on wing geometry and indicating the influence of antisymmetric loading at span station n on the downwash angle at span station ν. This equation is similar to equation (14) of reference 4 except that the antisymmetric influence coefficients are applicable for this loading, and the expression is summed for only three spanwise stations since the antisymmetric loading at the plane of symmetry is zero. The horizontal tail was then, in effect, considered as a wing having a twist distribution corresponding to the downwash, and the spanwise loading on the horizontal tail was computed by the method of reference 5. From this loading, the method of reference 6 was used to calculate the horizontal tail rolling-moment coefficient, which was then expressed in terms of wing dimensions.

[redacted]

REFERENCES

1. Cook, Woodrow L., Holzhauser, Curt A., and Kelly, Mark W.: The Use of Area Suction for the Purpose of Improving Trailing-Edge Flap Effectiveness on a 35° Sweptback Wing. NACA RM A53E06, 1953.

2. Kelly, Mark W., and Tolhurst, William H., Jr.: The Use of Area Suction to Increase the Effectiveness of a Trailing-Edge Flap on a Triangular Wing of Aspect Ratio 2. NACA RM A54A25, 1954.

3. Cook, Woodrow L., and Kelly, Mark W.: The Use of Area Suction for the Purpose of Delaying Separation of Air Flow at the Leading Edge of a 63° Swept-Back Wing - Effects of Controlling the Chordwise Distribution of Suction-Air Velocities. NACA RM A51J24, 1952.

4. DeYoung, John: Theoretical Symmetric Span Loading Due to Flap Deflection for Wings of Arbitrary Plan Form at Subsonic Speeds. NACA Rep. 1071, 1952.

5. DeYoung, John and Harper, Charles W.: Theoretical Symmetric Span Loading at Subsonic Speeds for Wings Having Arbitrary Plan Form. NACA Rep. 921, 1948.

6. DeYoung, John: Theoretical Antisymmetric Span Loading for Wings of Arbitrary Plan Form at Subsonic Speeds. NACA Rep. 1056, 1951.

7. Anon.: Flying Qualities of Piloted Airplanes. Spec. MIL-F-8785 (ASG), 1 Sept. 1954.

TABLE I.- AIRFOIL ORDINATES PARALLEL TO PLANE OF SYMMETRY OF THE 45° SWEPTBACK WING MODEL

x, percent chord	y, percent chord
0	0
.44	.631
.66	.761
1.10	.962
2.20	1.325
4.42	1.830
6.65	2.209
8.89	2.525
13.42	3.023
18.01	3.406
22.65	3.696
27.35	3.907
32.12	4.041
36.93	4.097
41.82	4.049
46.77	3.909
51.78	3.695
56.85	3.418
62.00	3.088
67.21	2.709
72.49	2.291
77.85	1.850
83.27	1.402
88.77	.947
94.35	.486
100	.019
Leading-edge radius: 0.475 percent chord	

[redacted]

TABLE II.- SPANWISE AND CHORDWISE LOCATIONS OF PRESSURE ORIFICES

Spanwise positions of orifices		Chordwise positions of orifices, percent streamwise chord[1]									
		Flaps undeflected		$\delta_f = 46°$		$\delta_f = 55°$		$\delta_f = 60°$		$\delta_f = 65°$	
Station no.	Percent semispan	Upper surface	Lower surface	Upper surface	Lower surface	Upper surface	Lower surface	Upper surface	Lower surface	Upper surface	Lower surface
1	24.0	0	---	0	---	0	---	0	---	0	---
2	41.2	.25	0.25	.26	0.26	.26	0.26	.27	0.27	.275	0.275
3	58.8	.5	.5	.52	.52	.53	.53	.54	.54	.55	.55
4	76.2	1.0	1.0	1.03	1.03	1.06	1.06	1.08	1.08	1.10	1.10
5	93.0	1.5	1.5	1.55	1.55	1.59	1.59	1.62	1.62	1.65	1.65
		2.5	2.5	2.59	2.59	2.66	2.66	2.70	2.70	2.75	2.75
		5.0	5.0	5.18	5.18	5.30	5.30	5.40	5.40	5.51	5.51
		7.5	7.5	7.77	7.77	7.97	7.97	8.10	8.10	8.26	8.26
		10.0	10.0	10.35	10.35	10.6	10.6	10.8	10.8	11.0	11.0
		15.0	15.0	15.5	15.5	15.9	15.9	16.2	16.2	16.5	16.5
		20.0	20.0	20.7	20.7	21.2	21.2	21.6	21.6	22.0	22.0
		30.0	30.0	31.1	31.1	31.9	31.9	32.4	32.4	33.0	33.0
		40.0	40.0	41.4	41.4	42.5	42.5	43.2	43.2	44.0	44.0
		50.0	50.0	51.8	51.8	53.0	53.0	54.0	54.0	55.1	55.1
		60.0	60.0	62.1	62.1	63.6	63.6	64.8	64.8	66.1	66.1
		70.0	70.0	72.5	72.5	74.2	74.2	75.6	75.6	77.1	77.1
		80.0	80.0	77.2	82.5	79.6	84.3	80.9	85.4	82.6	87.2
		90.0	90.0	81.2	91.2	83.3	92.1	84.8	92.7	86.7	93.6
		95.0	95.0	81.6	95.6	83.9	96.0	85.4	95.3	87.3	96.9
		97.5	97.5	81.9	97.8	84.3	97.9	86.0	98.2	87.8	98.6
				82.3		84.8		86.5		88.9	
				82.7		85.6		87.3		89.4	
				83.0		86.6		88.1		89.9	
				84.1		93.3		94.2		95.2	
				92.2		96.6		97.1		97.4	
				96.0		98.0		98.5		98.9	
				98.0							

[1]With the trailing-edge flaps deflected, the orifice positions are given in percent of the foreshortened chord.

TABLE III.- VALUES OF $C_{Q_{f_{crit}}}$, $C_{P_{f_{crit}}}$, AND s/c' FOR AREA SUCTION ON THE VARIOUS FLAP CONFIGURATIONS TESTED; $\alpha = 0^\circ$

Flap span	Flap deflection, deg	s/c'	$C_{Q_{f_{crit}}}$	$C_{P_{f_{crit}}}$
0.12 to 0.50 b/2	46	0.057	0.0007	-2.85
	55	.062	.0010	-3.90
	60	.064	.0012	-4.78
	65	.066	.0014	-4.93
0.12 to 0.66 b/2	46	.057	.0011	-3.21
	55	.062	.0012	-3.95
	60	.064	.0013	-4.18
	65	.066	.0016	-4.65
0.12 to 0.83 b/2	46	.057	.0013	-3.03
	55	.062	.0016	-3.90

TABLE IV.- FLOW COEFFICIENTS WITH SUCTION ON FLAP AND WING LEADING EDGE

$\delta_f = 60^\circ$, η_f = 0.12 to 0.50 b/2				$\delta_f = 60^\circ$, η_f = 0.12 to 0.66 b/2			
α	C_{Q_f}	$C_{Q_{le}}$	$C_{P_{le}}$	α	C_{Q_f}	$C_{Q_{le}}$	$C_{P_{le}}$
0	0.0011	0	0	0	0.0011	0	0
2	.0011	0	0	4	.0013	0	0
4	.0011	0	0	6	.0013	.0017	-16.4
6	.0011	.0013	-12.5	8	.0013	.0020	-23.0
8	.0011	.0014	-16.5	10	.0013	.0022	-24.3
10	.0012	.0016	-24.5	12	.0013	.0022	-30.8
12	.0012	.0018	-27.1	14	.0013	.0022	-33.8
14	.0012	.0023	-31.7	16	.0013	.0023	-36.5
16	.0012	.0024	-38.4	18	.0013	.0025	-36.5
18	.0012	.0026	-30.6				

[redacted]

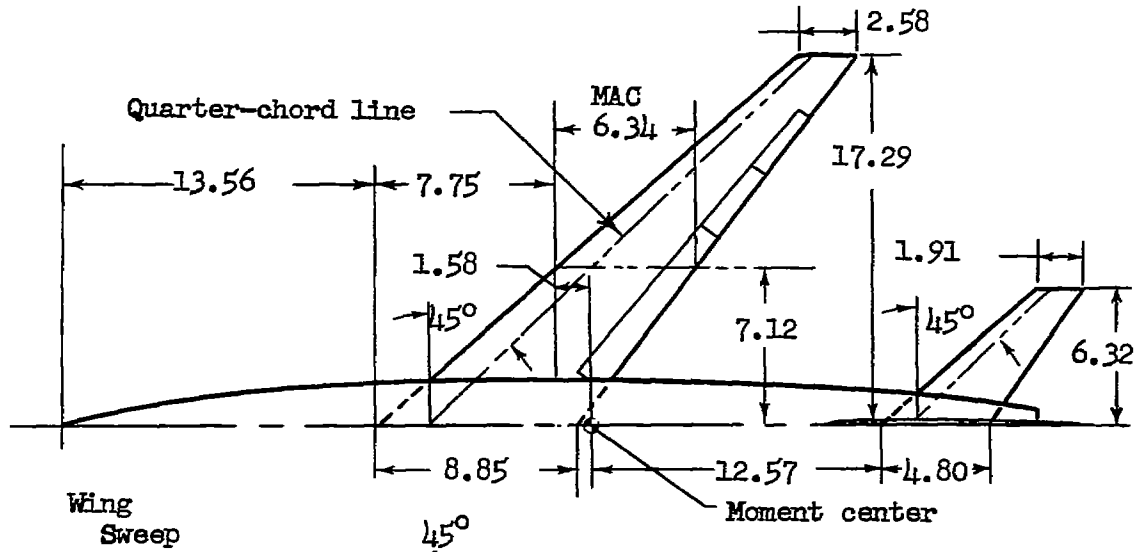

Wing	
Sweep	45°
Aspect ratio	6.0
Taper ratio	0.292
Twist	0°
Dihedral	0°
Area, sq ft	198.8
Thickness ratio	.082
Horizontal tail	
Sweep	45°
Dihedral	0°
Area, sq ft	42.5
Vertical tail	
Sweep	45.6°
Area, sq ft	35.0
Fuselage	
Fineness ratio	10.5
Radius at station d	$2.016\left[1-\left(\frac{d}{23}-1\right)^2\right]^{3/4}$ ft

All dimensions in feet, unless otherwise noted

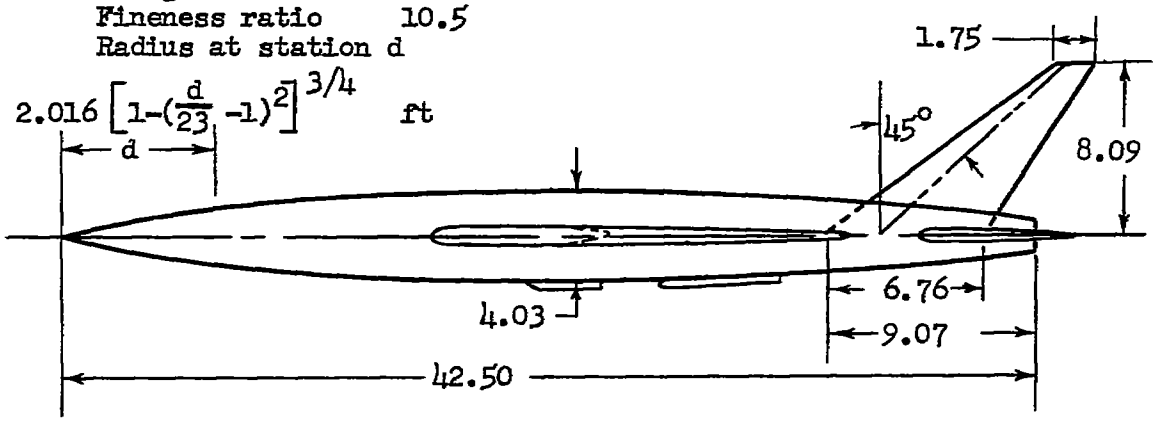

Figure 1.- Geometric characteristics of the model.

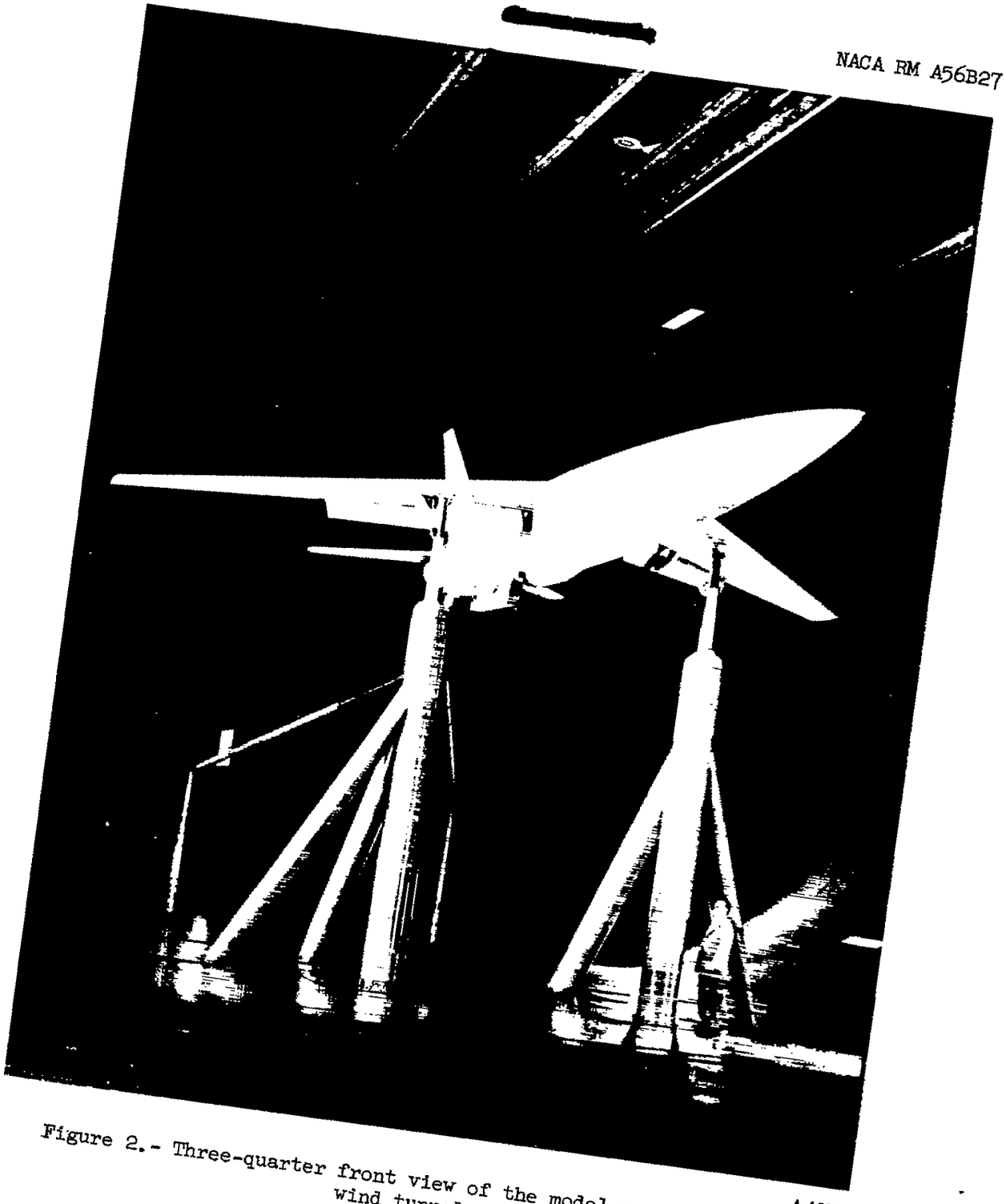

A-18816

Figure 2.- Three-quarter front view of the model mounted in the wind tunnel.

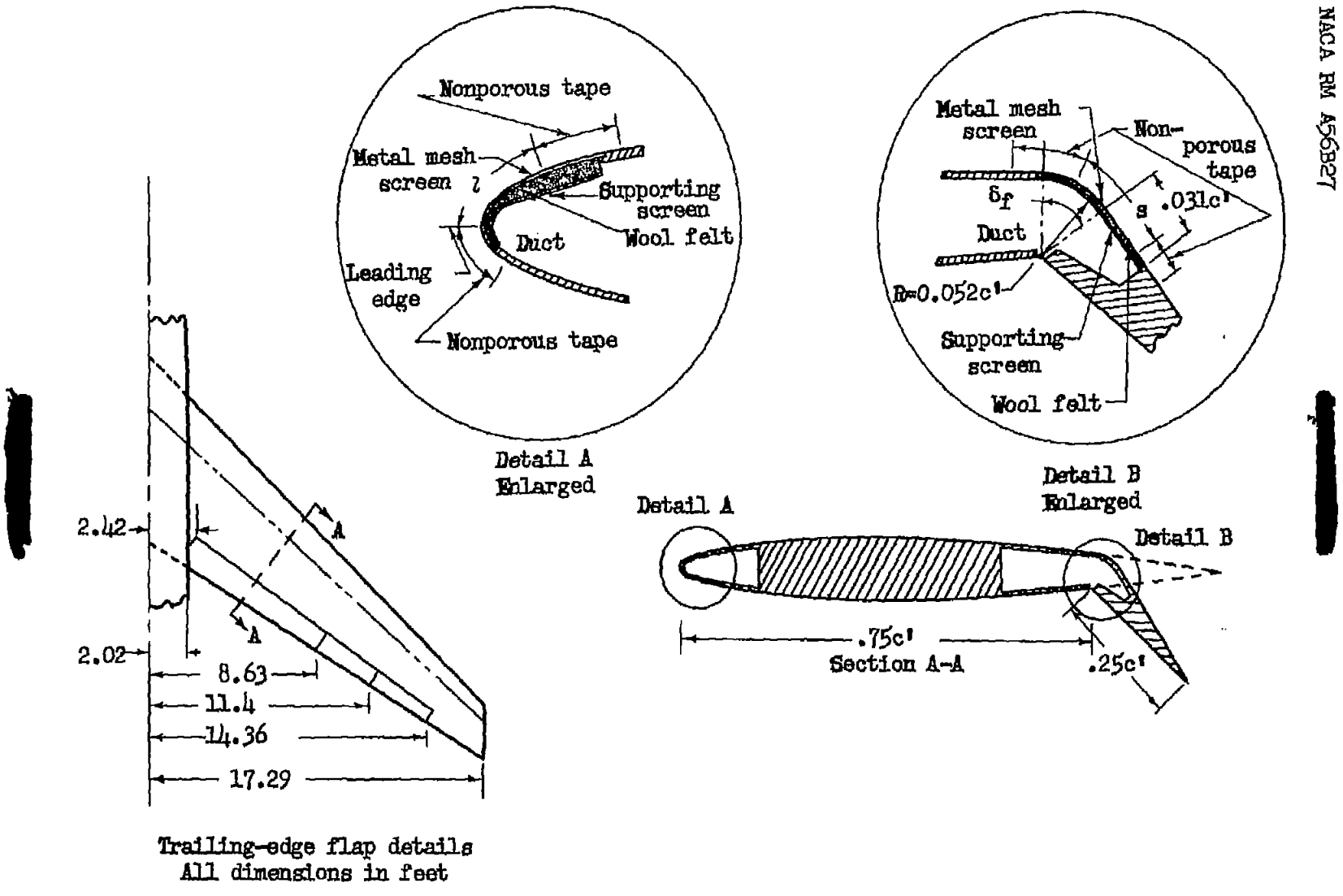

Figure 3.- Details of the flap and leading edge of the model.

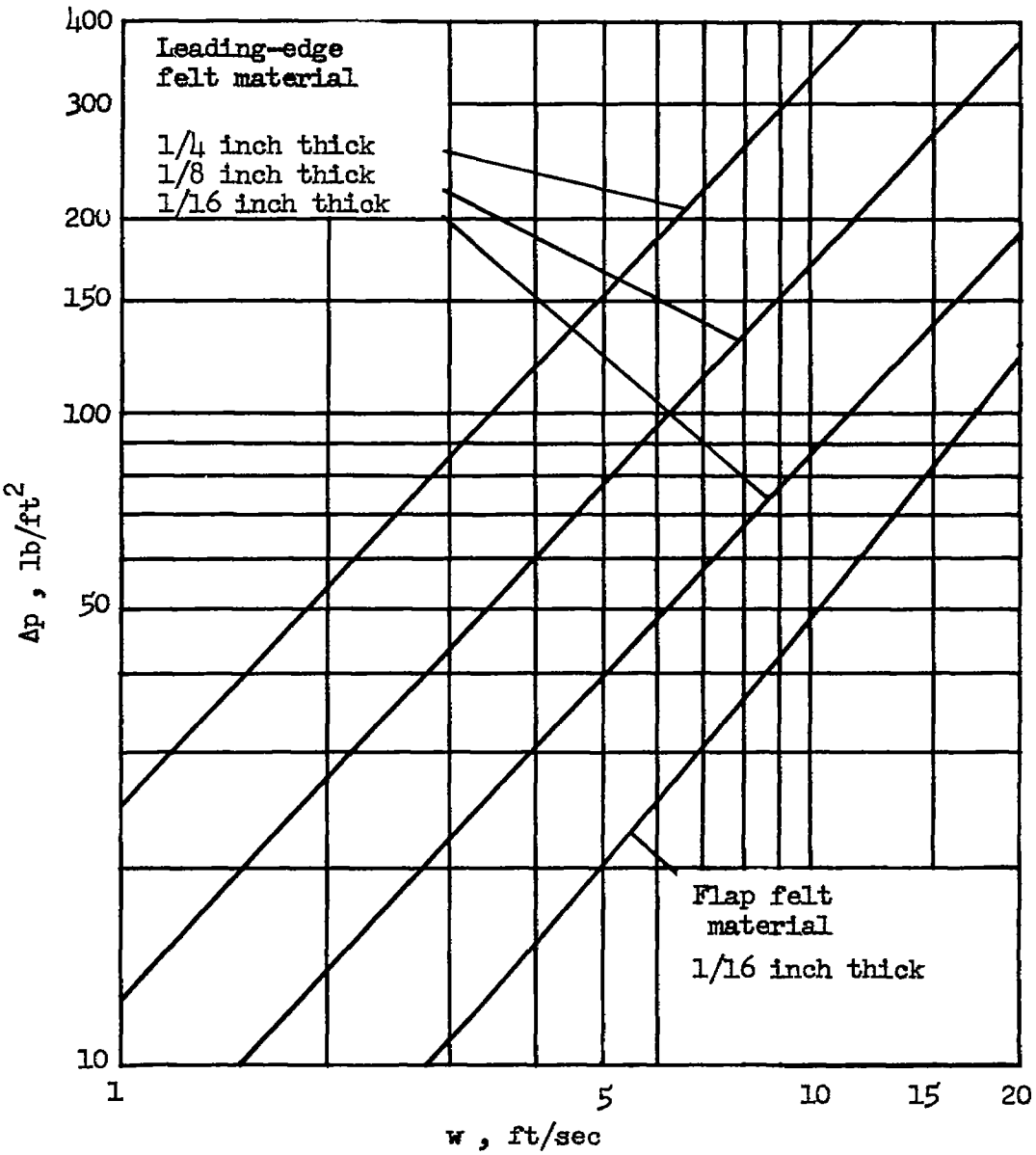

Figure 4.- Porosity characteristics of the wool felt material used for boundary-layer control.

[redacted]

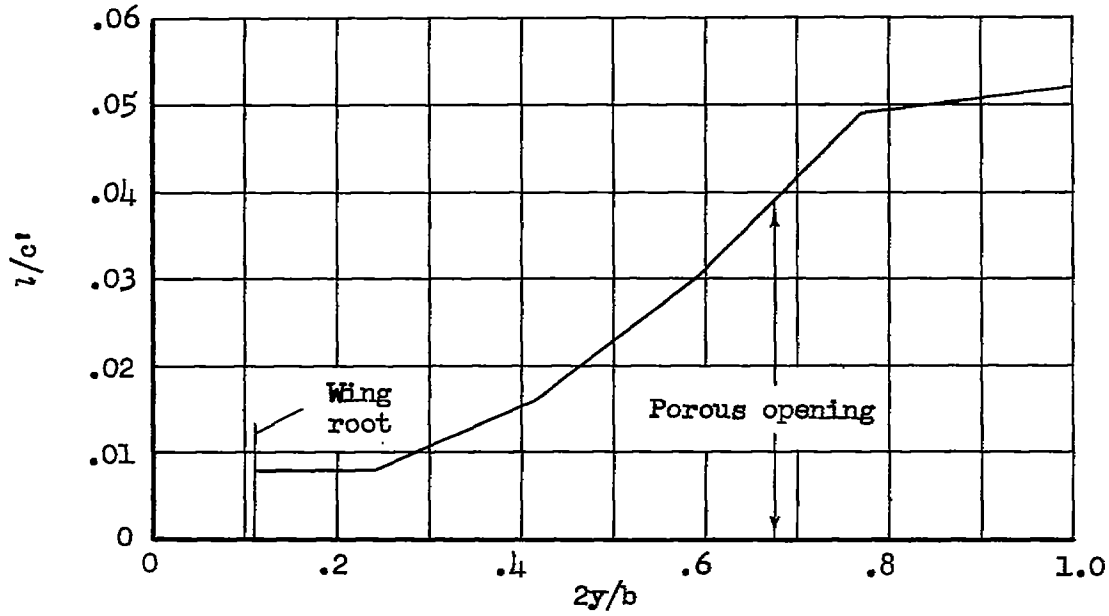

(a) Spanwise variation of chordwise extent of porous area at the wing leading edge.

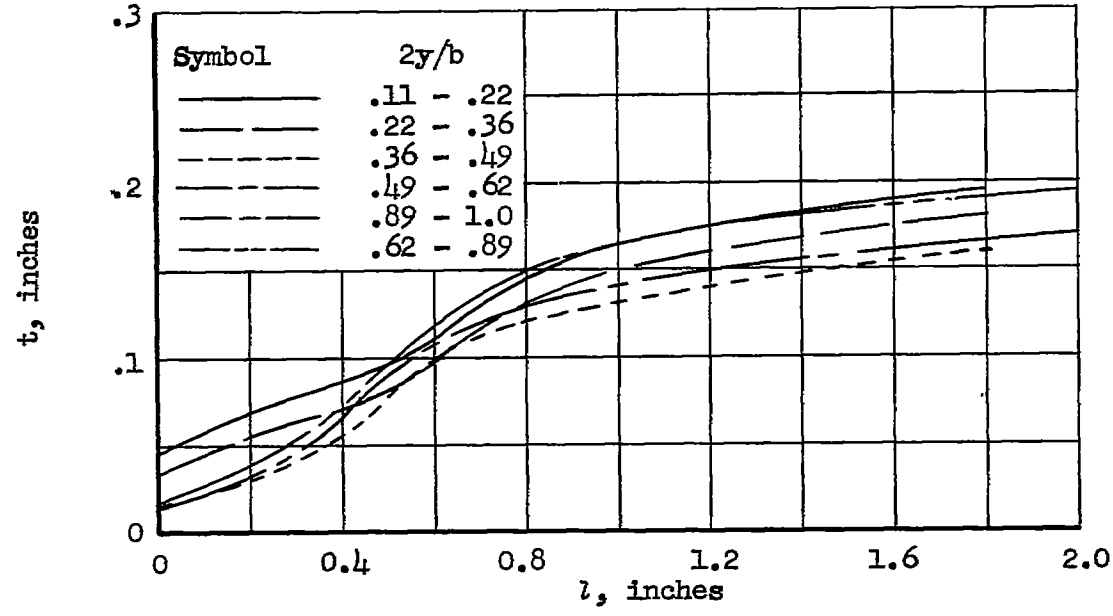

(b) Thickness variation of the felt backing used in the wing leading edge.

Figure 5.- Characteristics of the porous area at the wing leading edge.

[redacted]

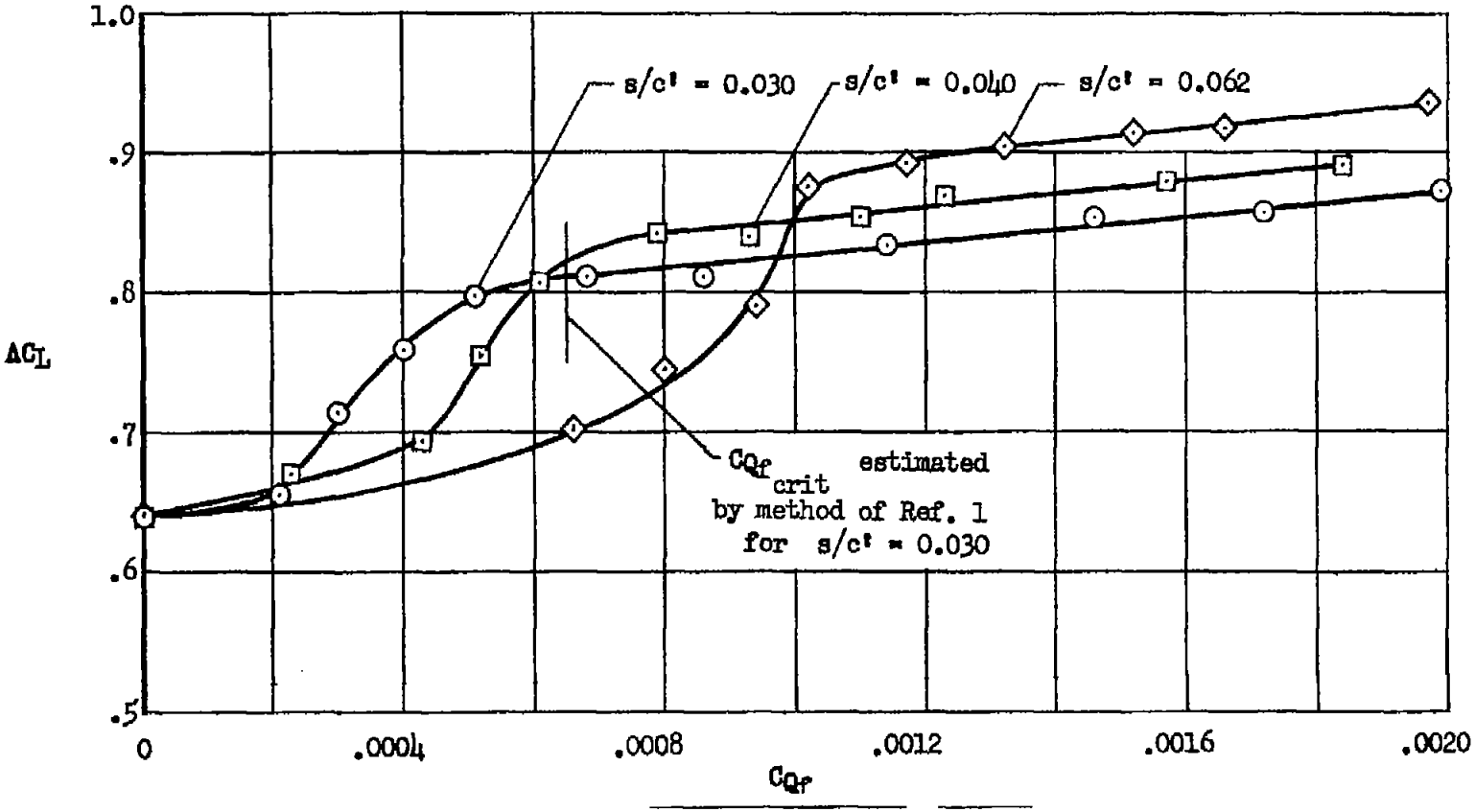

Figure 6.- Effect of flow coefficient on the flap lift coefficient increment for various chordwise extents of porous area; $\alpha = 0.4^\circ$, $\delta_f = 55^\circ$, flap span from 0.12 to 0.66 b/2, wing leading edge sealed.

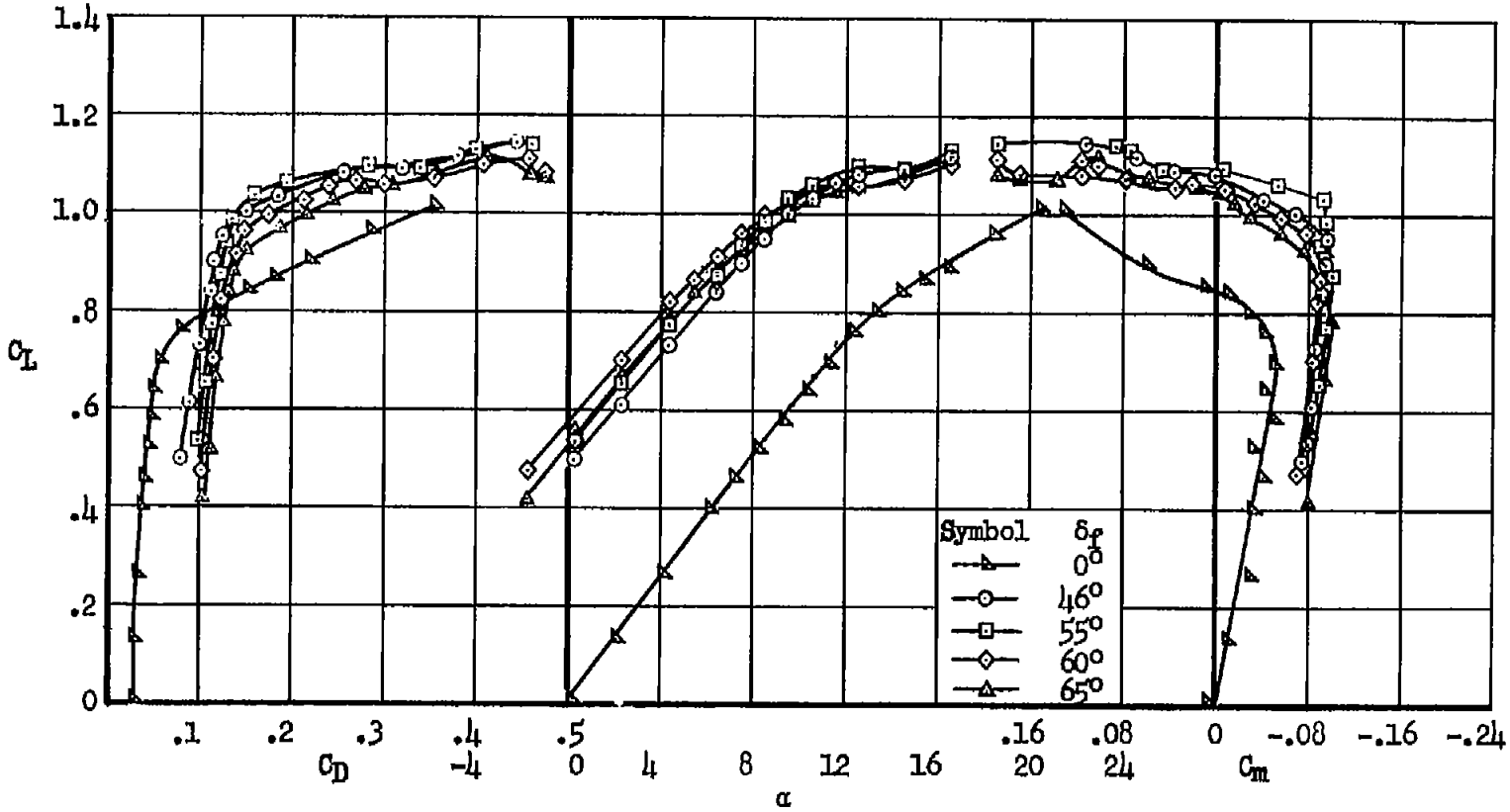

(a) Flap span extending from 0.12 to 0.50 b/2.

Figure 7.- Aerodynamic characteristics of the model at various flap deflections without boundary-layer control on the flaps; wing leading edge sealed.

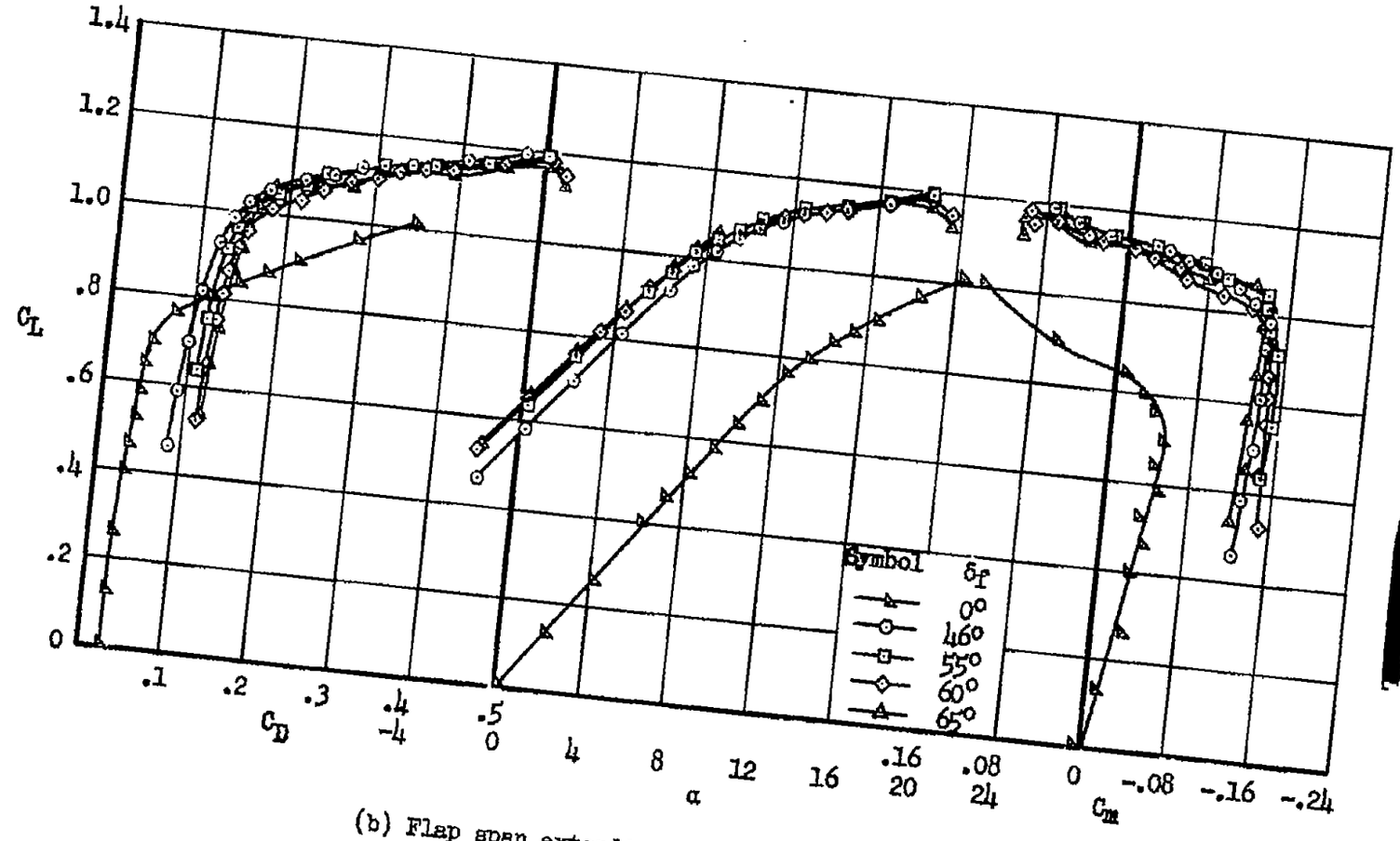

(b) Flap span extending from 0.12 to 0.66 b/2.

Figure 7.- Continued.

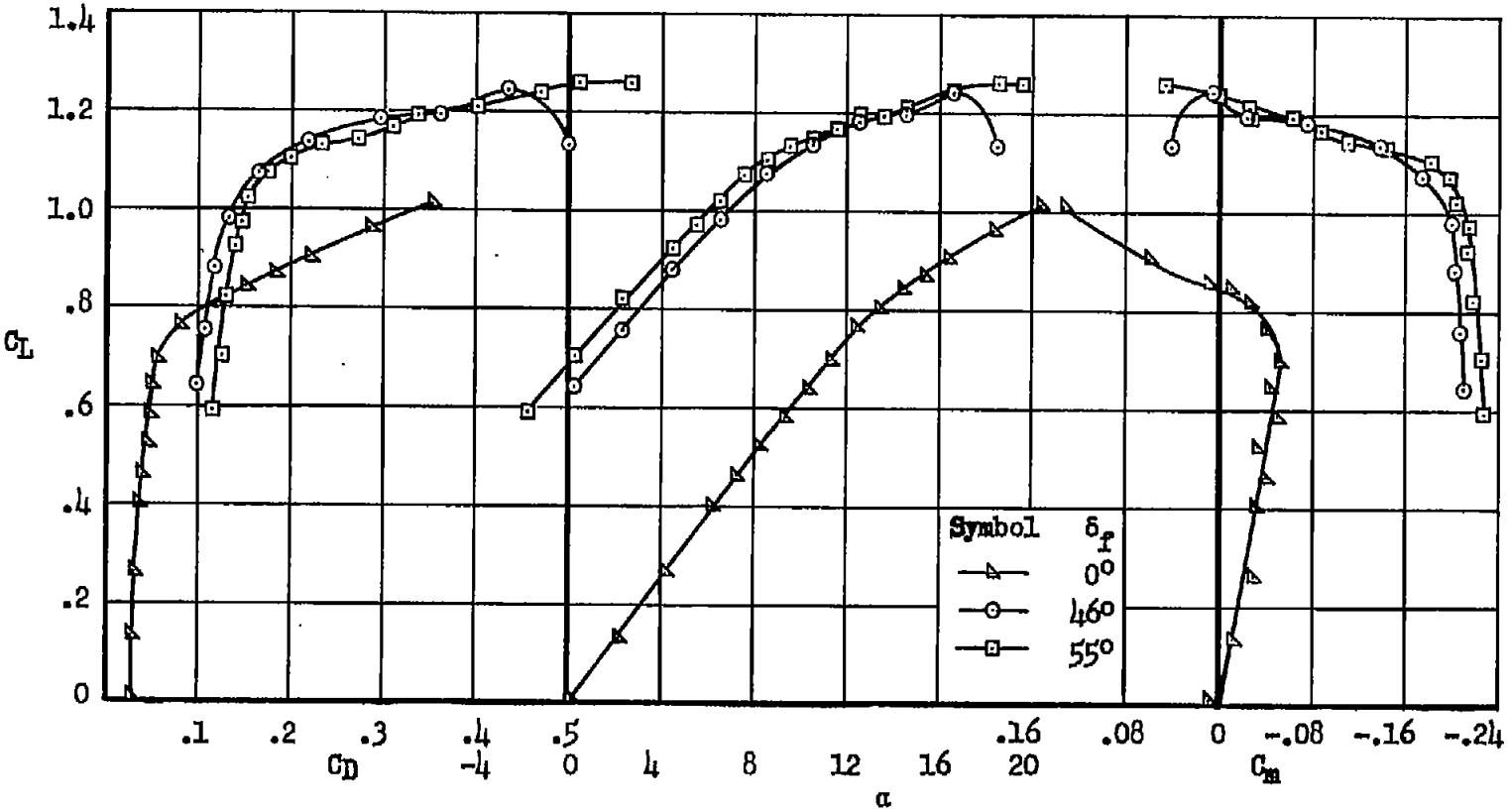

(c) Flap span extending from 0.12 to 0.83 b/2.

Figure 7.- Concluded.

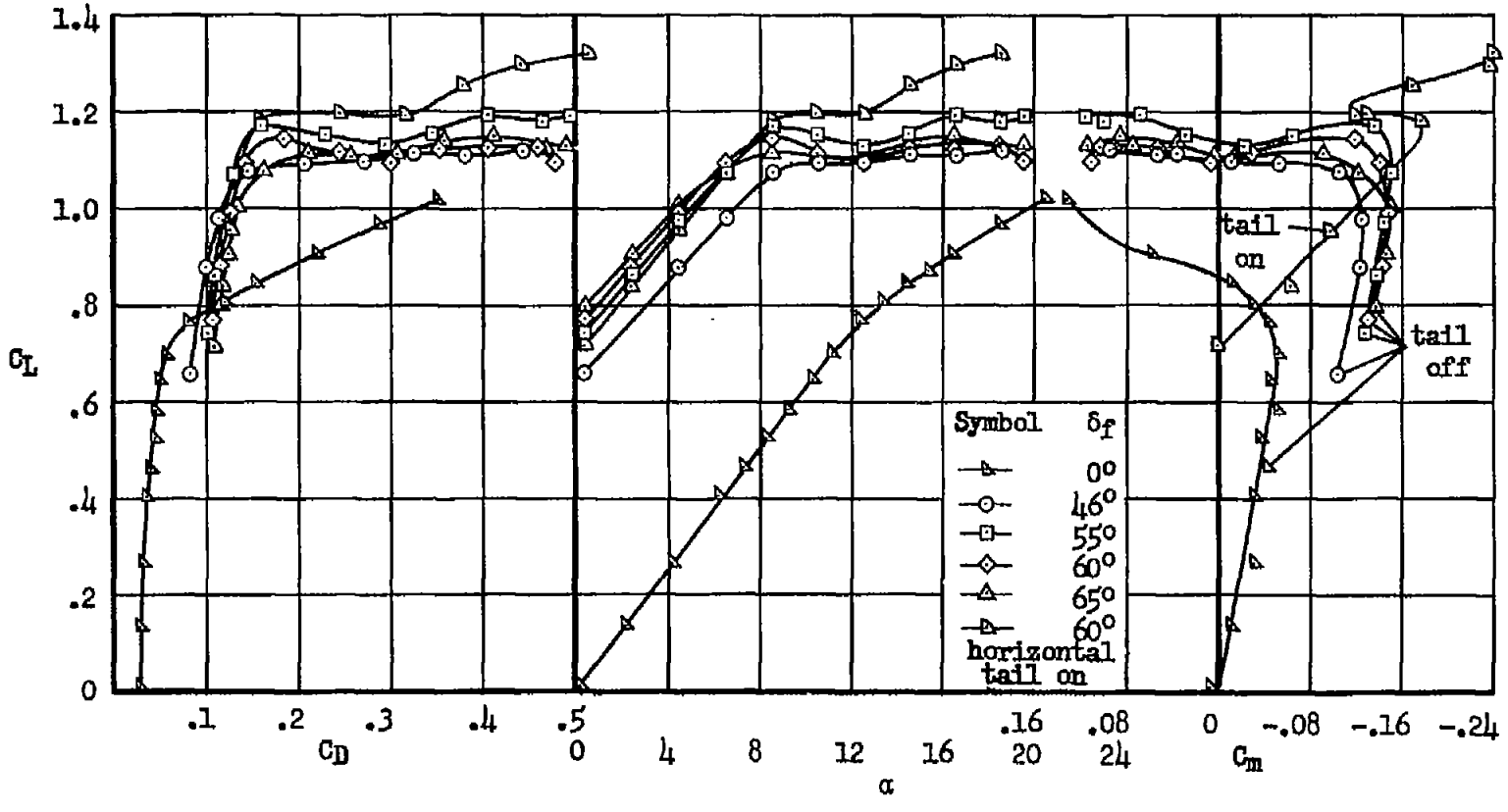

(a) Flap span extending from 0.12 to 0.50 b/2.

Figure 8.- Aerodynamic characteristics of the model at various flap deflections with boundary-layer control on the flaps; wing leading edge sealed.

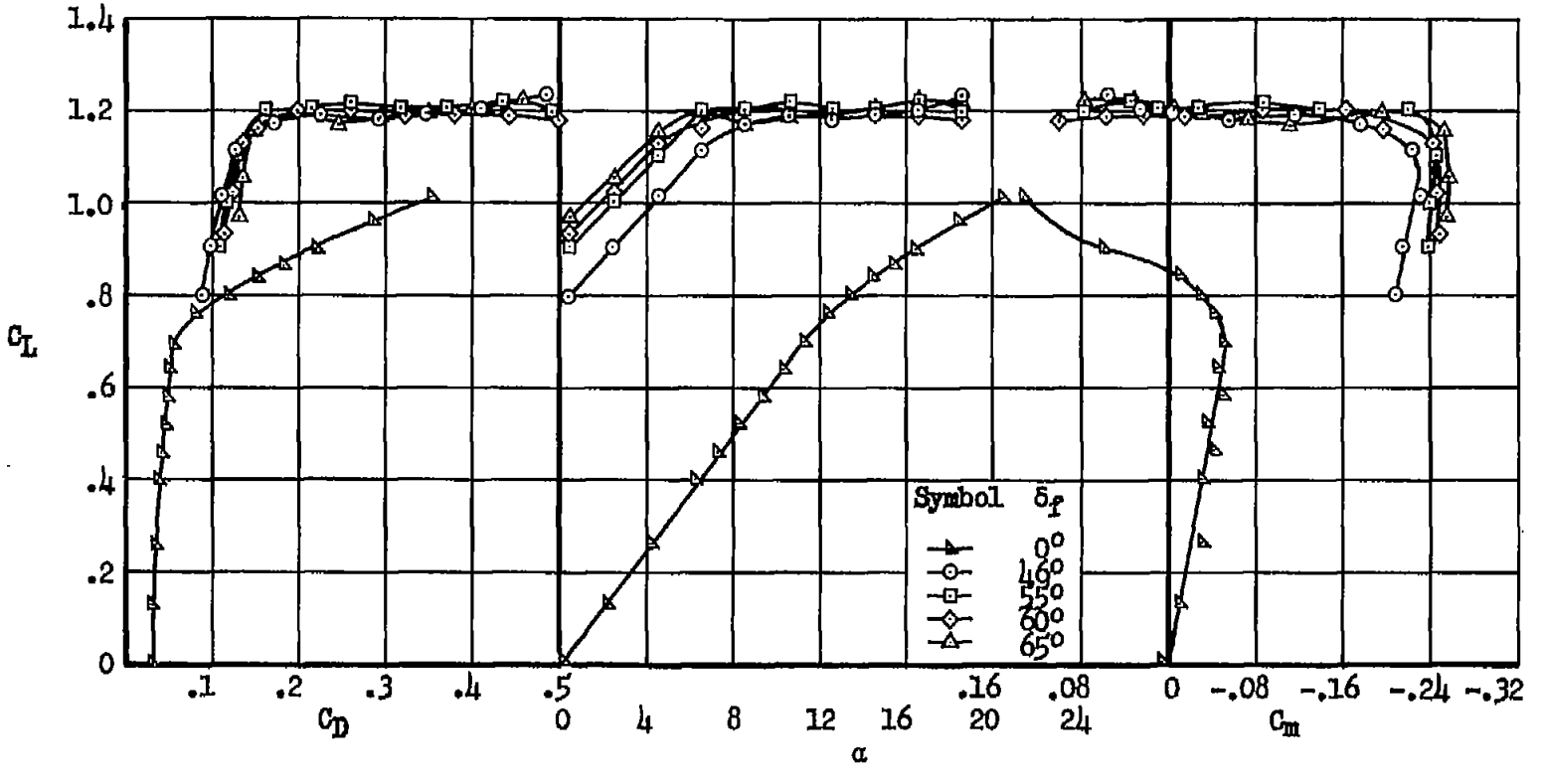

(b) Flap span extending from 0.12 to 0.66 b/2.

Figure 8.- Continued.

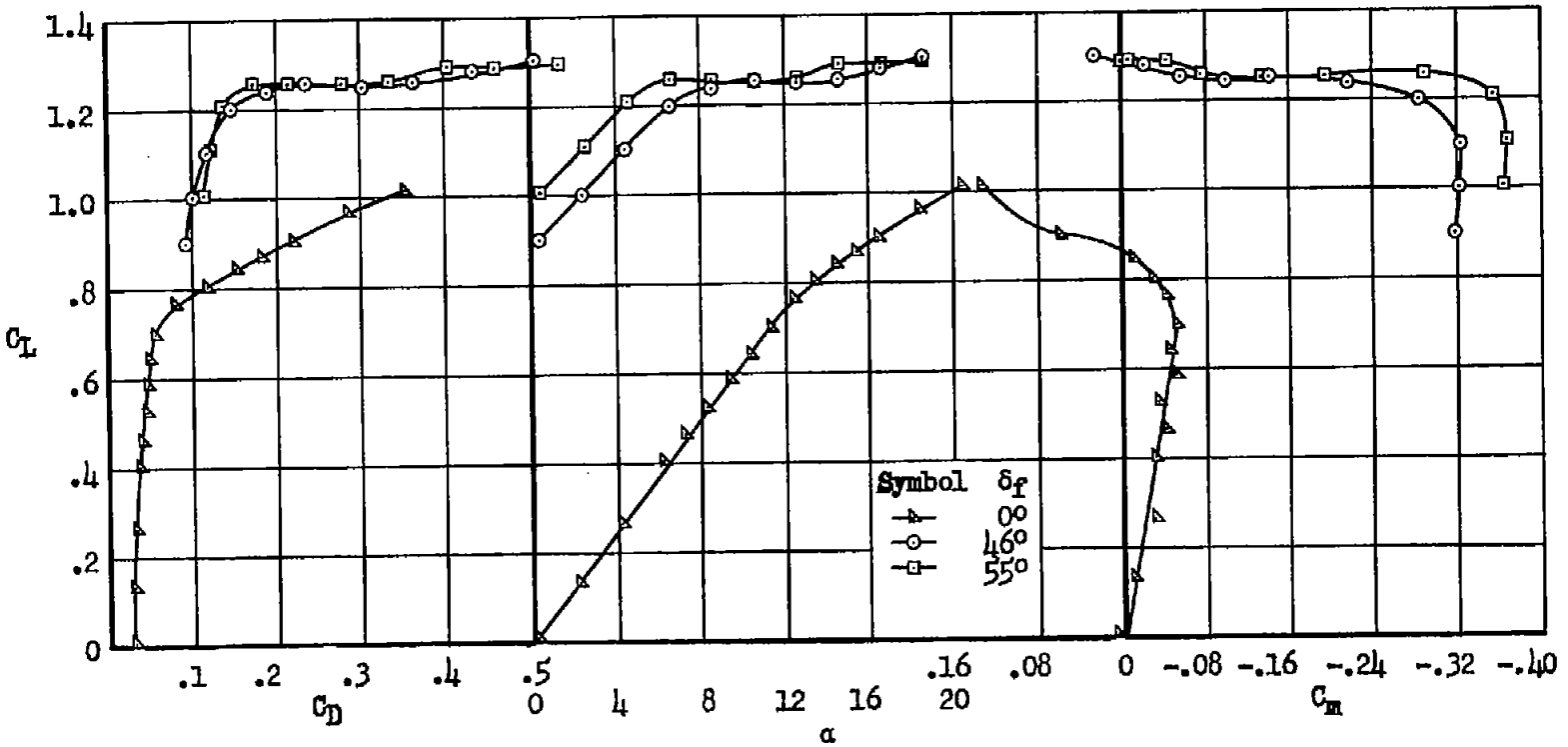

(c) Flap span extending from 0.12 to 0.83 b/2.

Figure 8.- Concluded.

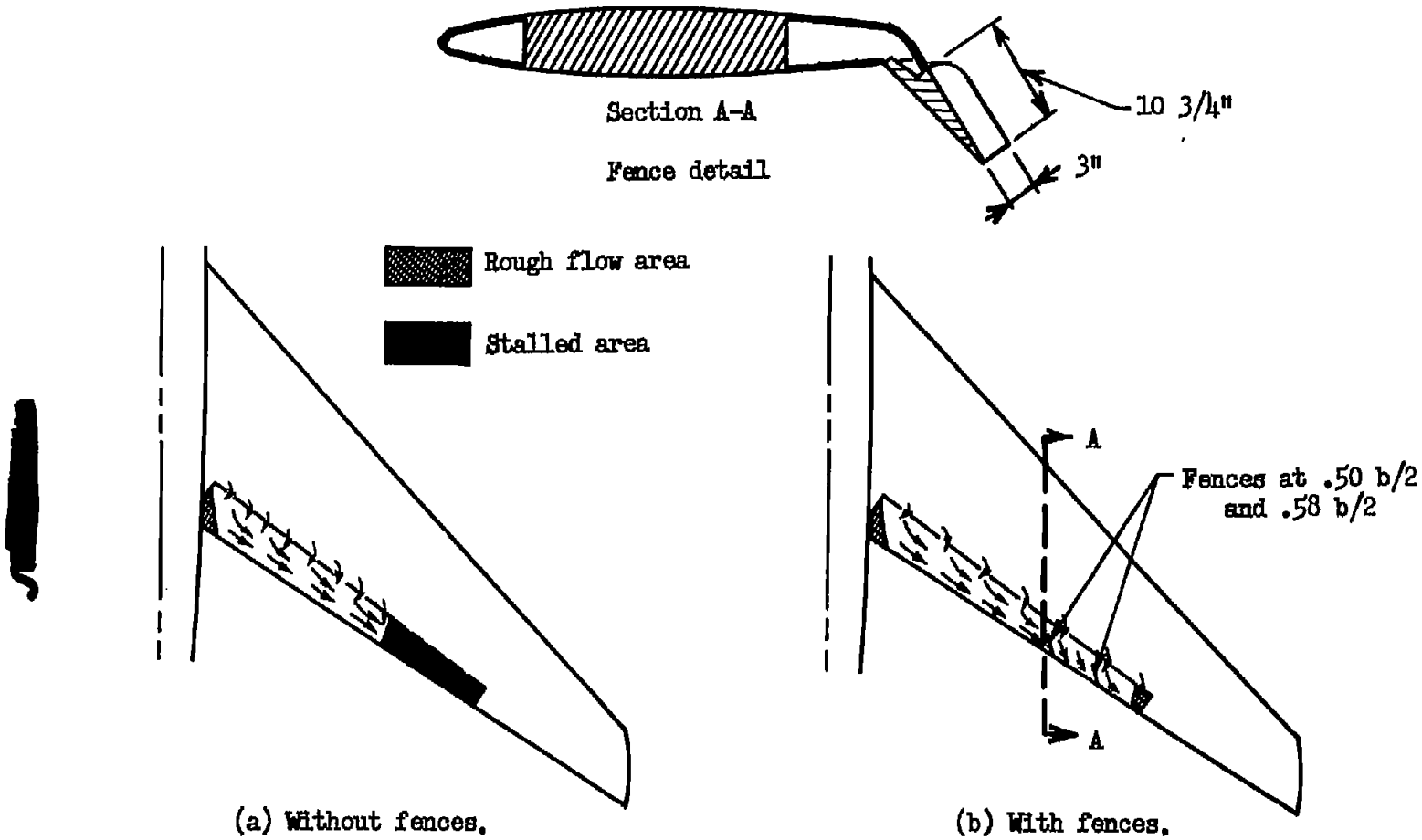

Figure 9.- Tuft study of the flow over the flaps with suction on the flap; $\delta_f = 65^\circ$, flap span from 0.12 to 0.66 b/2.

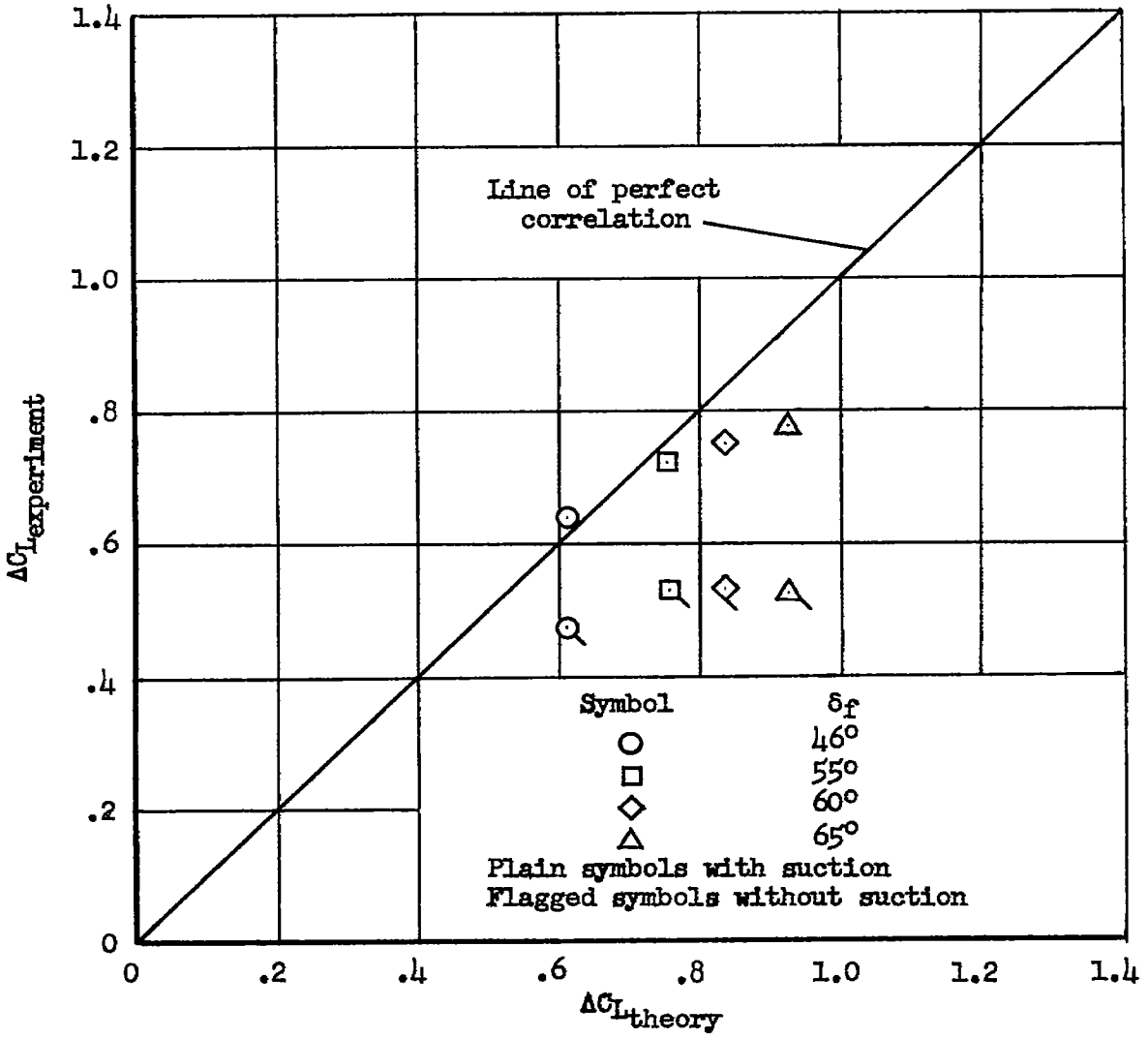

(a) Flap span from 0.12 to 0.50 b/2.

Figure 10.- Comparison of experimental lift attained by the trailing-edge flaps with and without suction and the theoretical lift calculated by the method of reference 4; $\alpha = 0^\circ$.

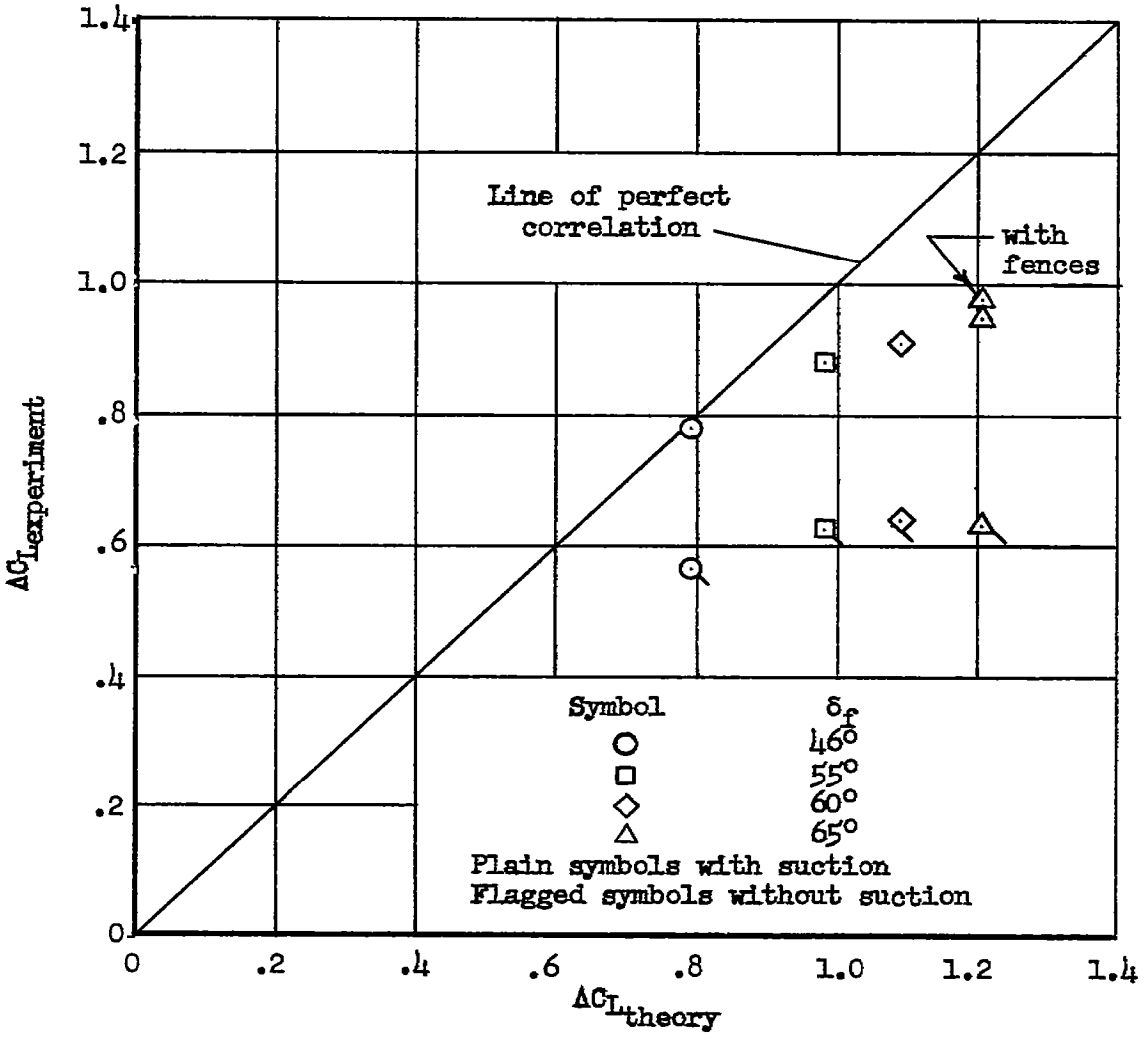

(b) Flap span from 0.12 to 0.66 b/2.

Figure 10.- Continued.

[redacted]

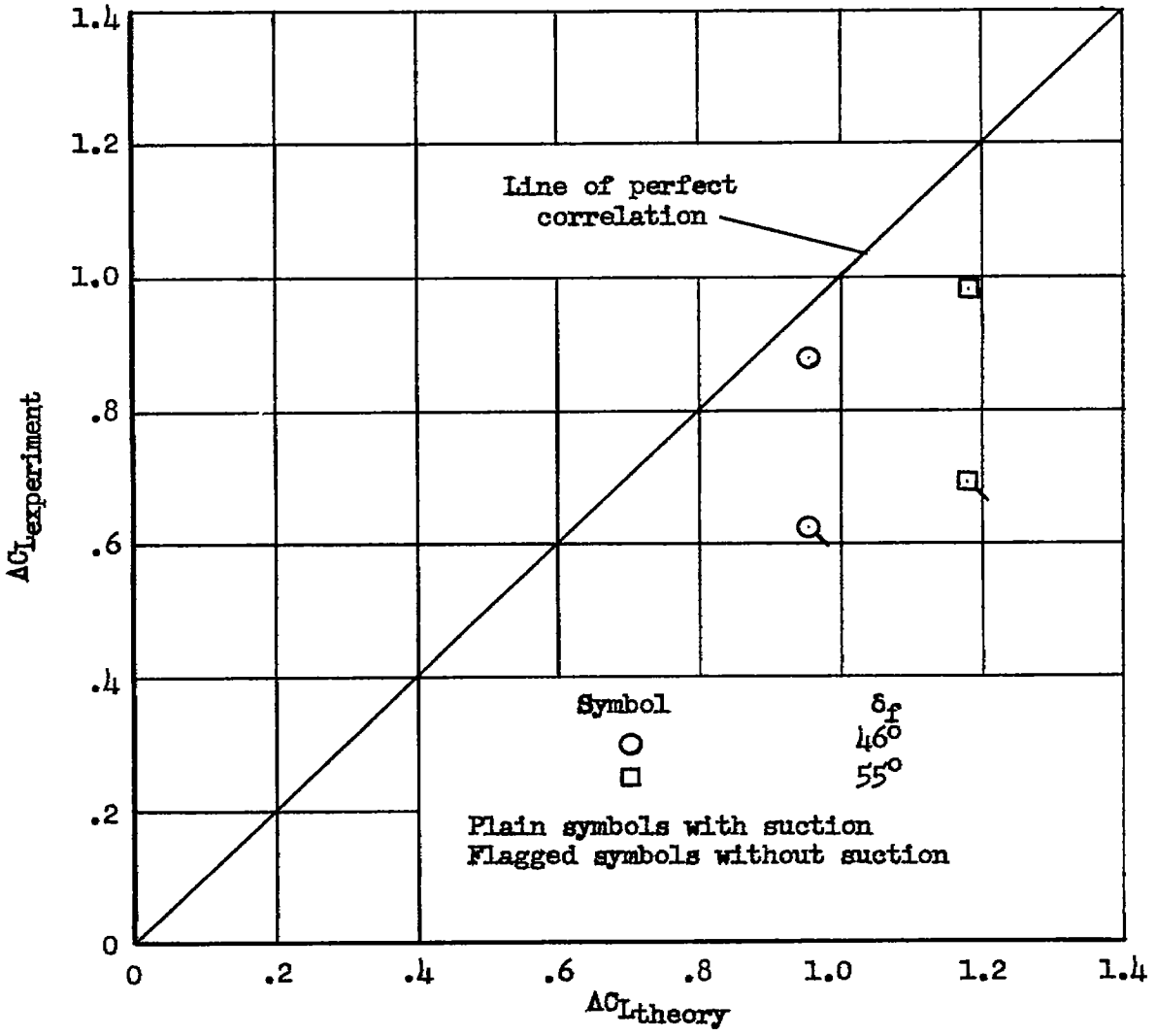

(c) Flap span from 0.12 to 0.83 b/2.

Figure 10.- Concluded.

[redacted]

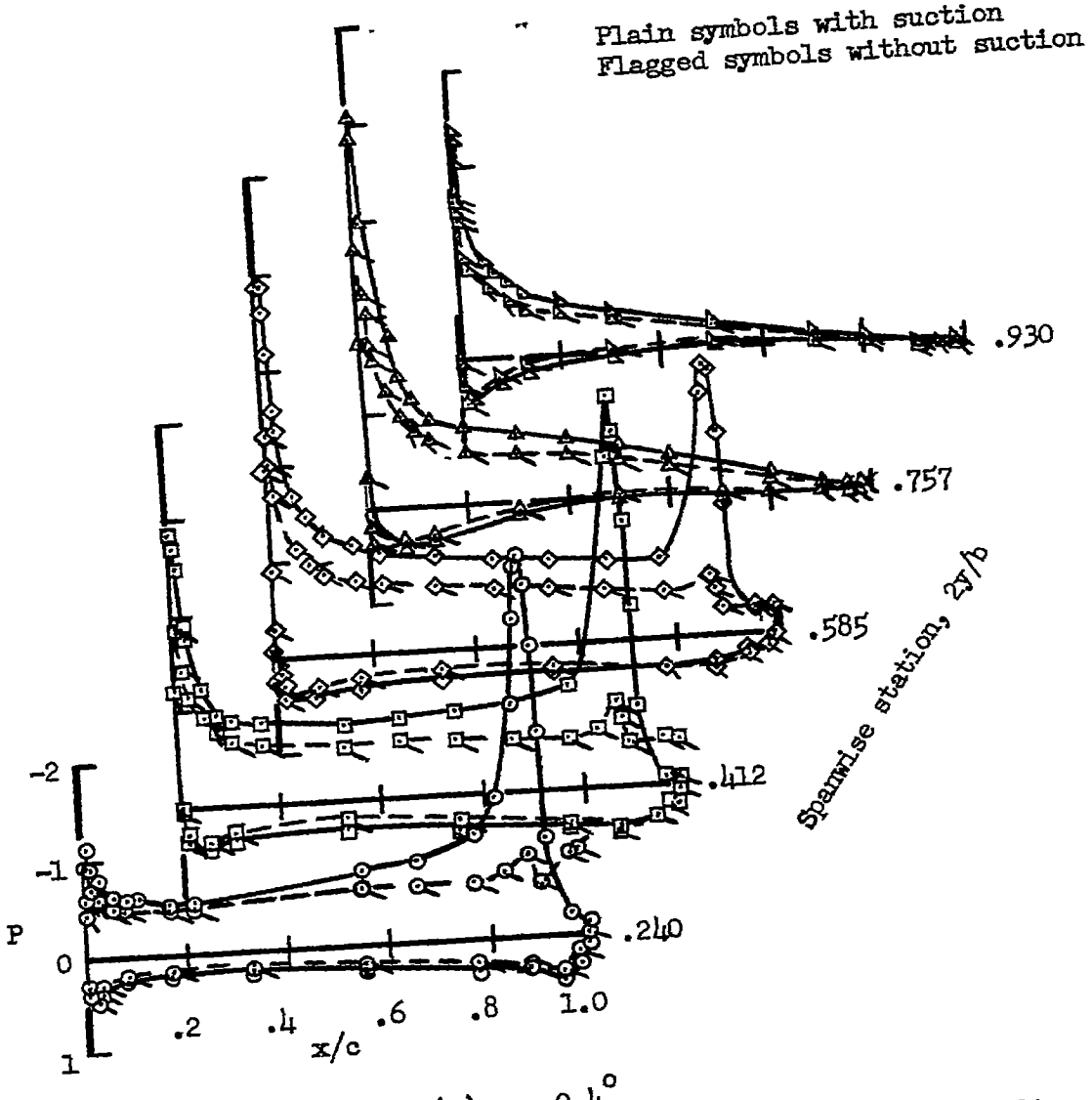

(a) $\alpha = 0.4^{\circ}$

Figure 11.- Comparison at five spanwise stations of the pressure distributions for the wing with and without suction on the flap; $\delta_f = 60^{\circ}$, flap span from 0.12 to 0.66 b/2.

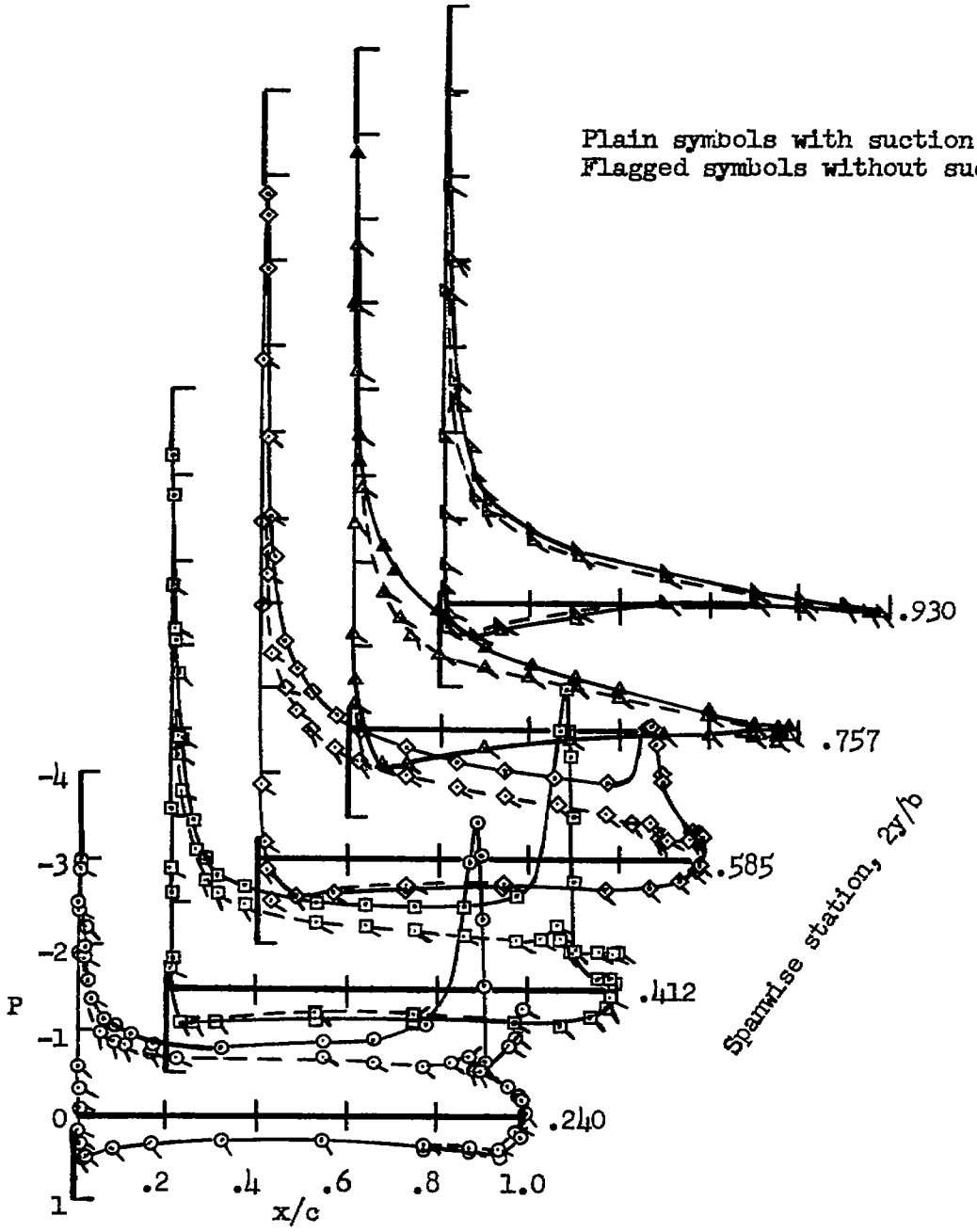

(b) $\alpha = 4.5^{\circ}$

Figure 11.- Continued

[redacted]

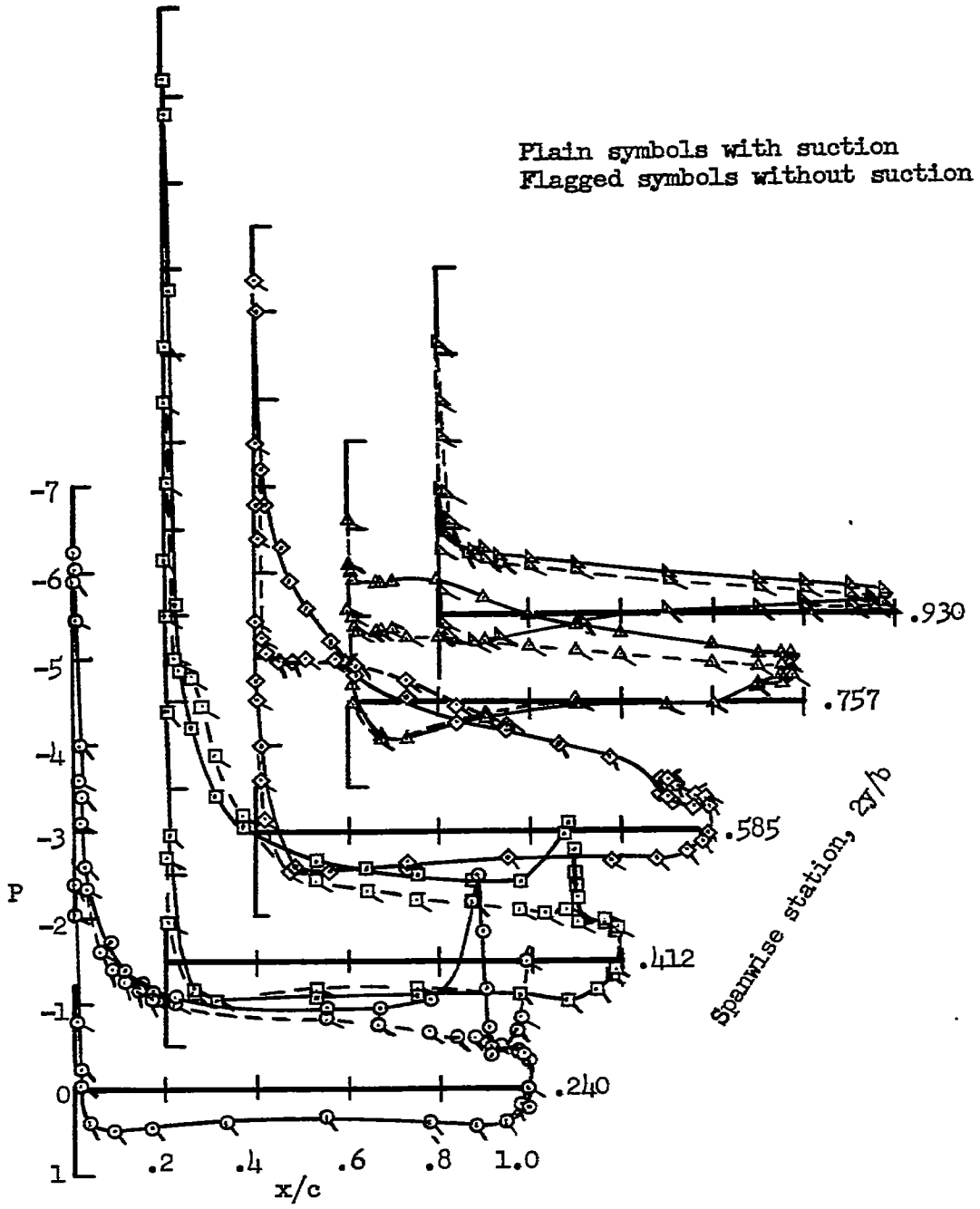

(c) $\alpha = 8.6^{\circ}$

Figure 11.- Continued.

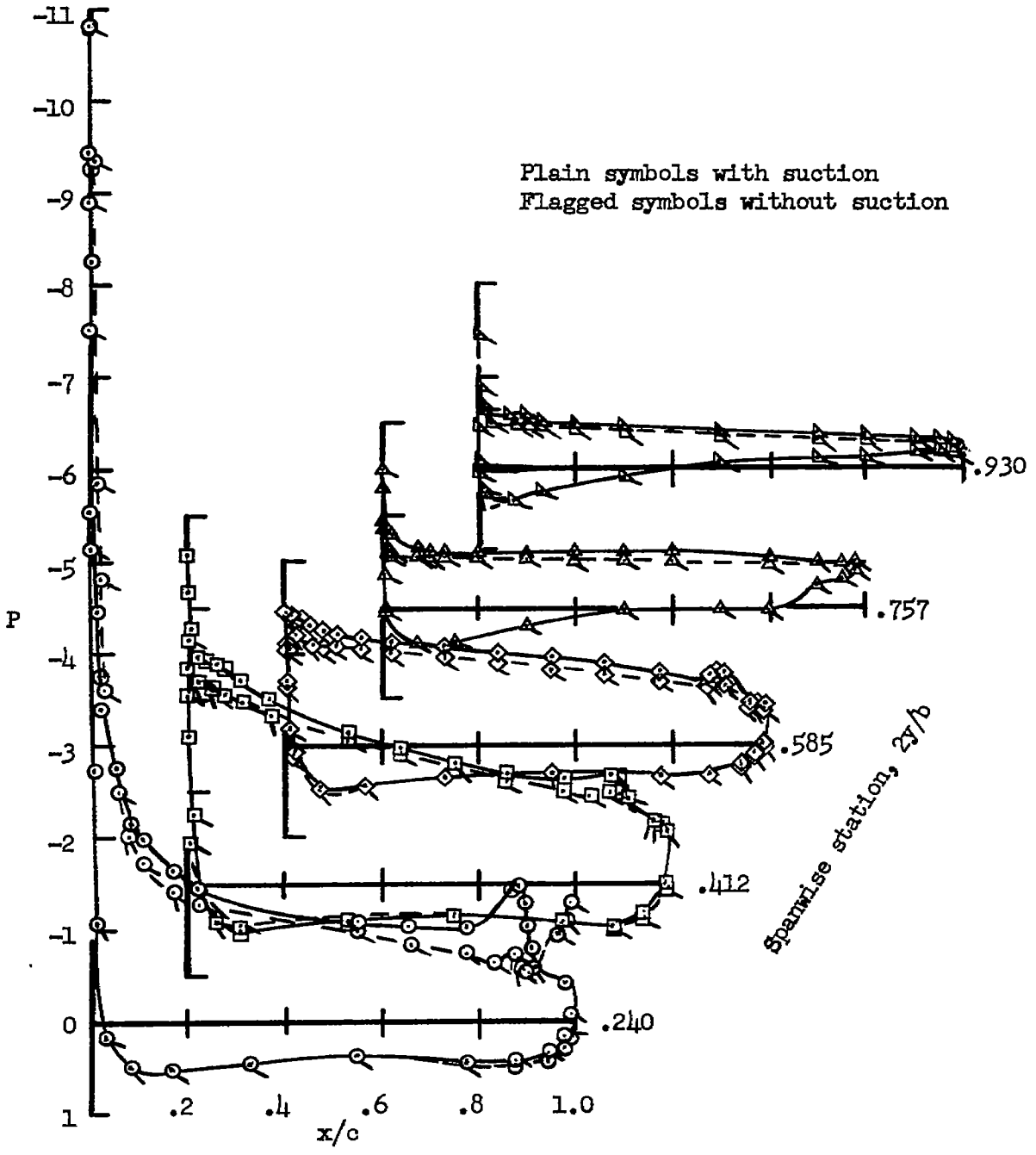

(d) $\alpha = 12.6^{\circ}$

Figure 11.- Continued.

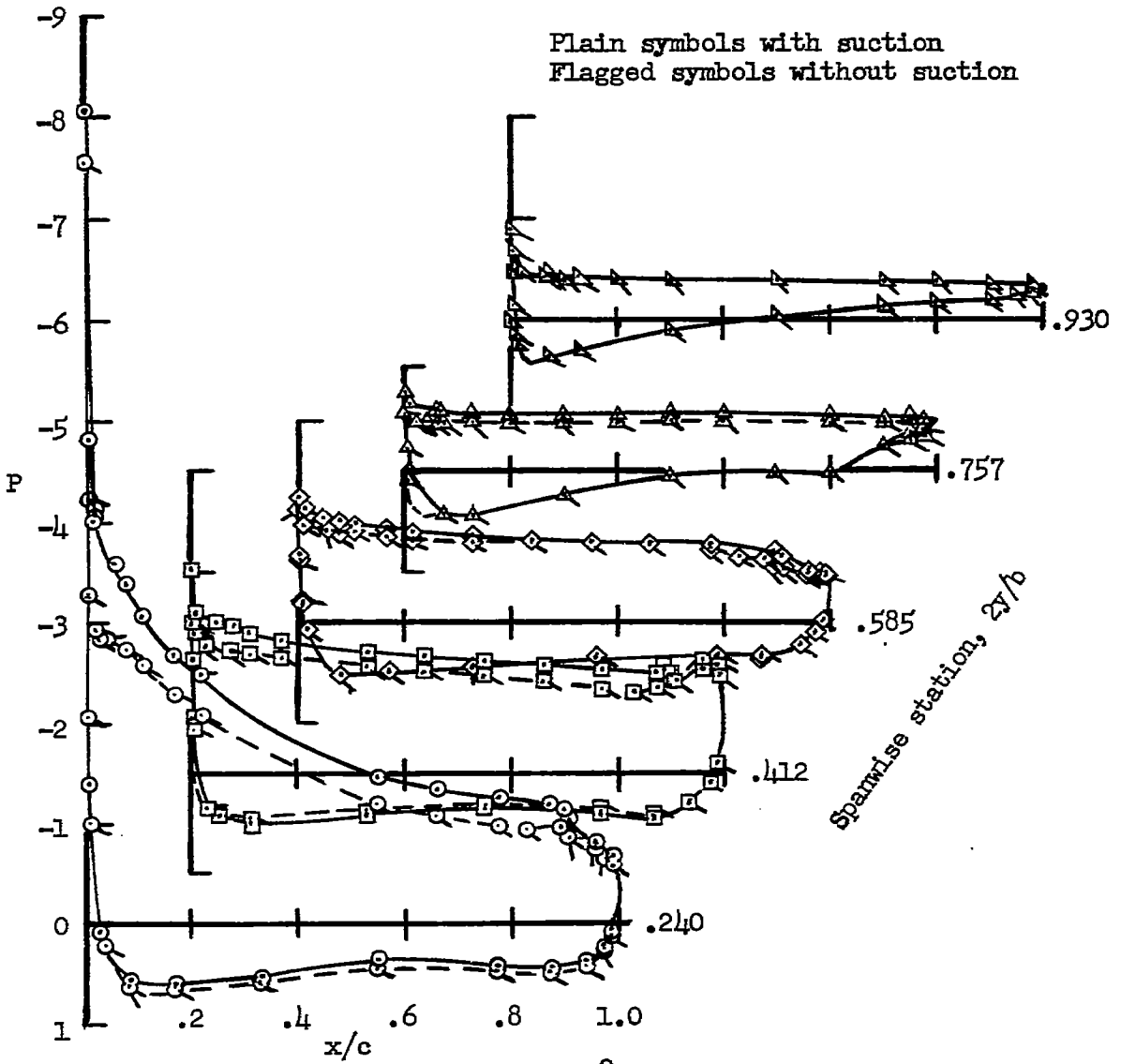

(e) $\alpha = 16.7^{\circ}$

Figure 11.- Concluded.

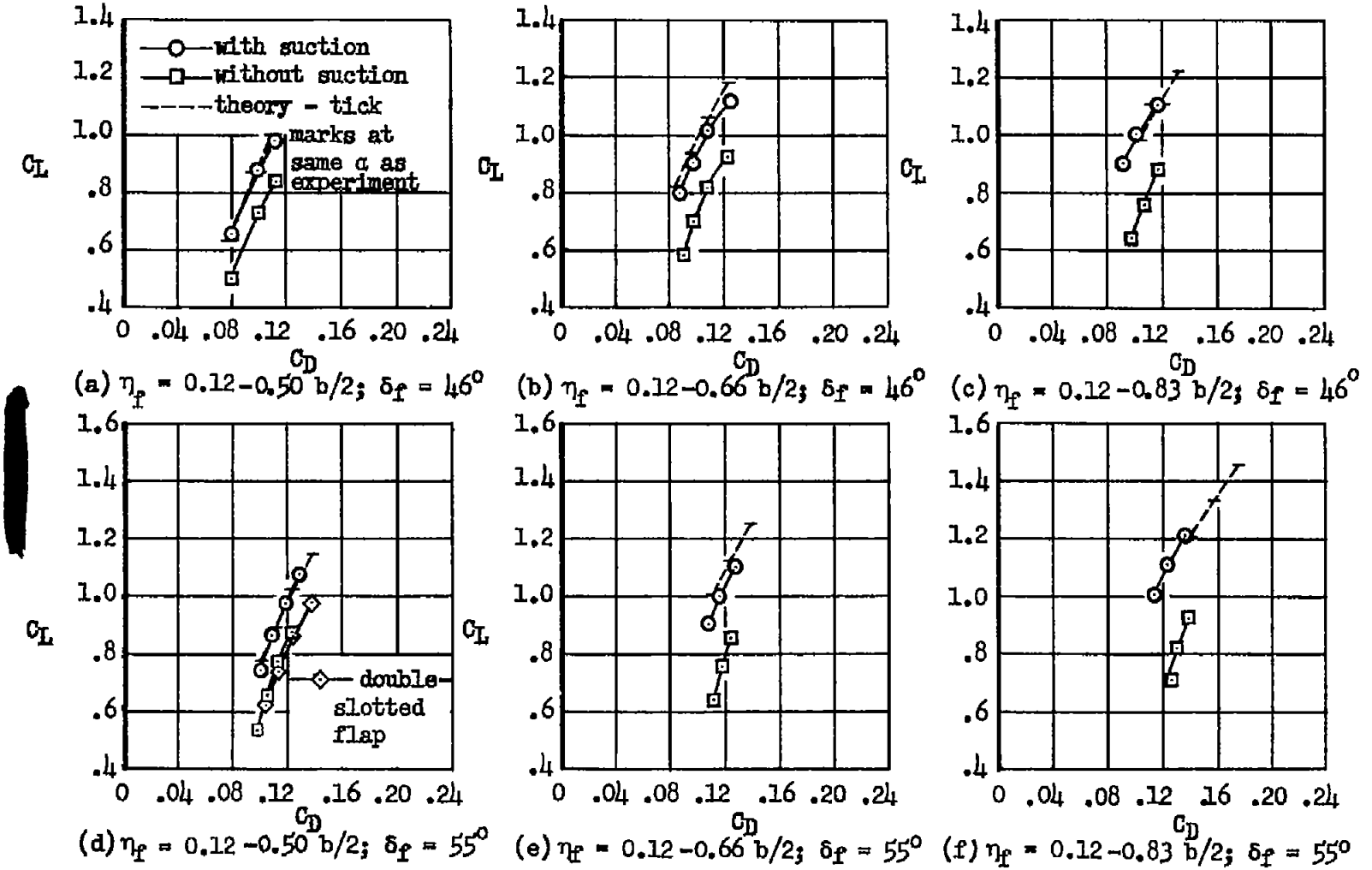

Figure 12.- Comparison of experimental lift-drag polars with and without suction to the theoretical polars obtained by the method of reference 5.

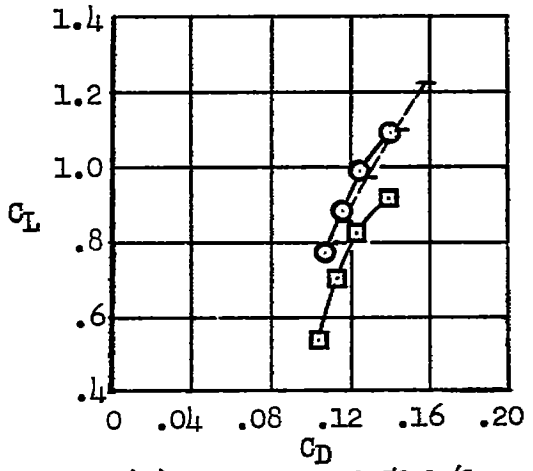

(g) η_f = 0.12 -0.50 b/2
δ_f = 60°

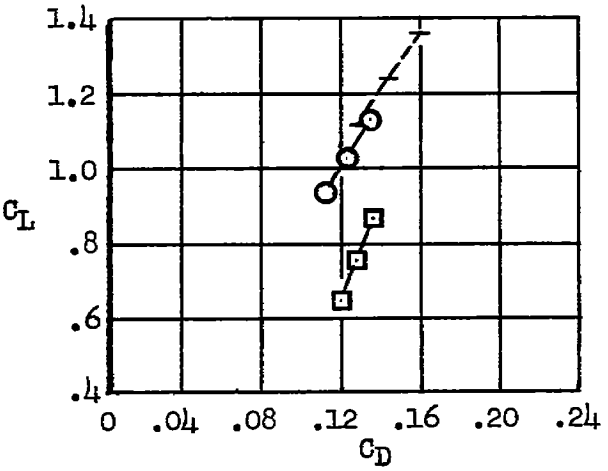

(h) η_f = 0.12 -0.66 b/2
δ_f = 60°

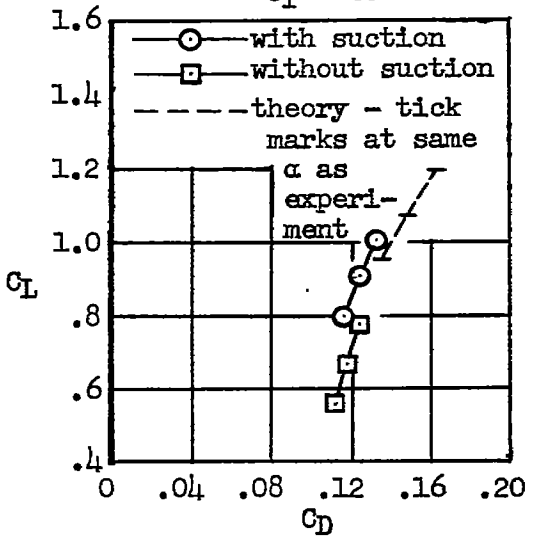

(i) η_f = 0.12 -0.50 b/2
δ_f = 65°

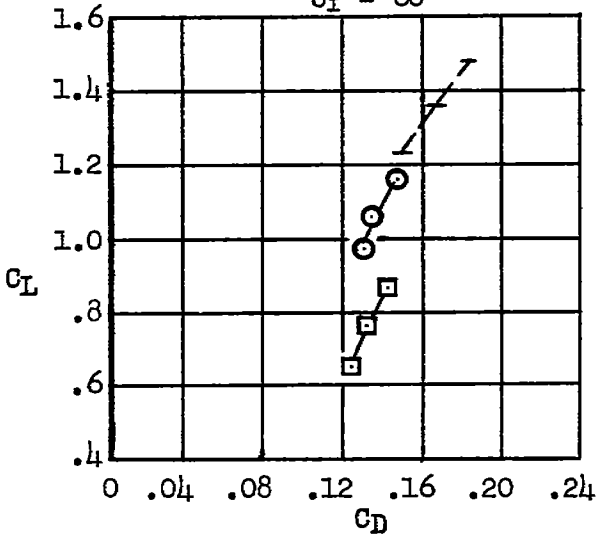

(j) η_f = 0.12 -0.66 b/2
δ_f = 65°

Figure 12.- Concluded.

[redacted]

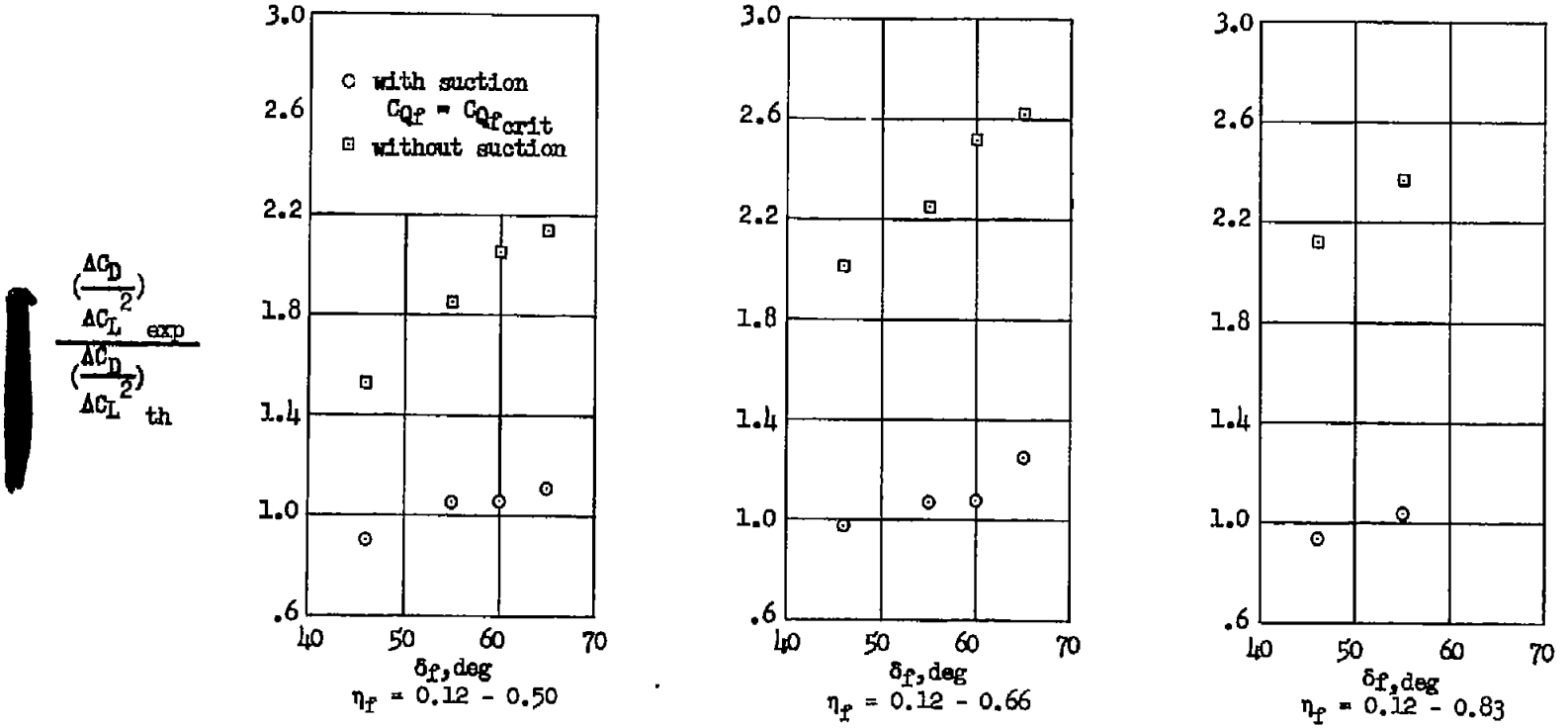

Figure 13.- Effect of suction on the drag parameter $(\Delta C_D/\Delta C_L^2)_{exp}/(\Delta C_D/\Delta C_L^2)_{th}$ for all flap configurations at zero angle of attack.

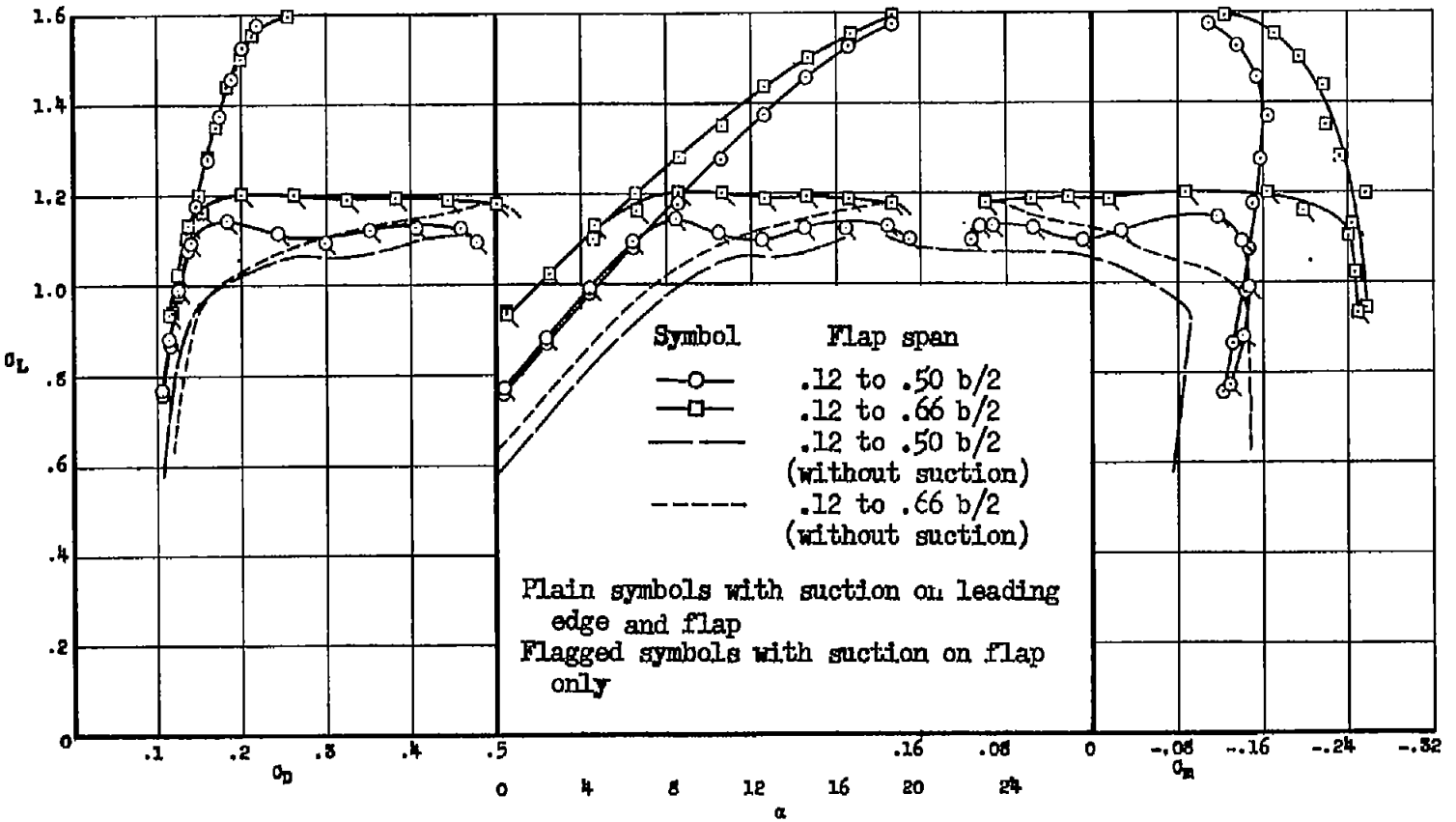

Figure 14.- Effect of leading-edge area suction on the aerodynamic characteristics of the model with area suction applied to each of two flap spans.

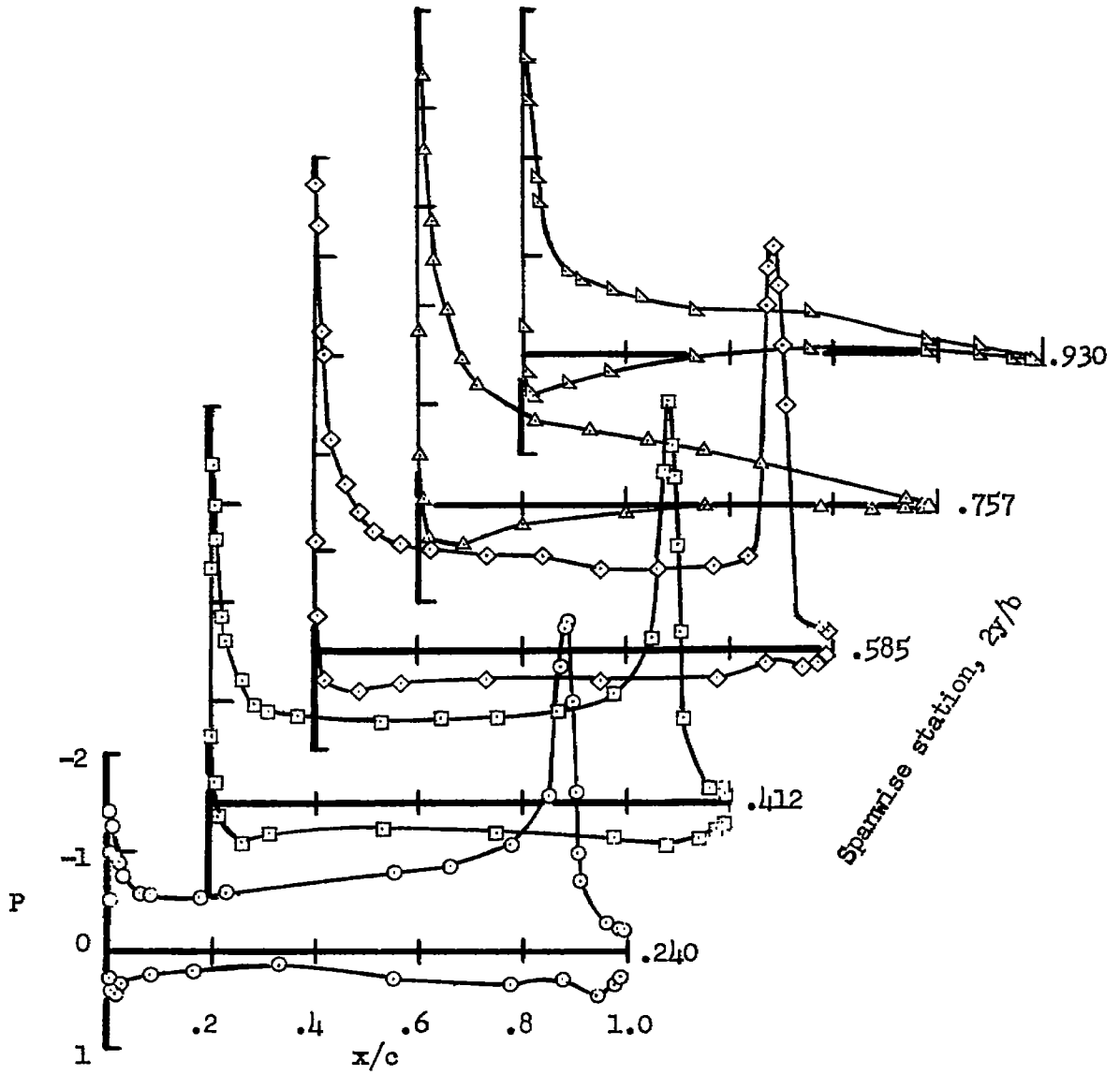

(a) $\alpha = 0.4$

Figure 15.- Pressure distributions on the wing of the model with boundary-layer control applied to the flap and leading edge; $\delta_f = 60^\circ$, flap span from 0.12 to 0.66 b/2.

[redacted]

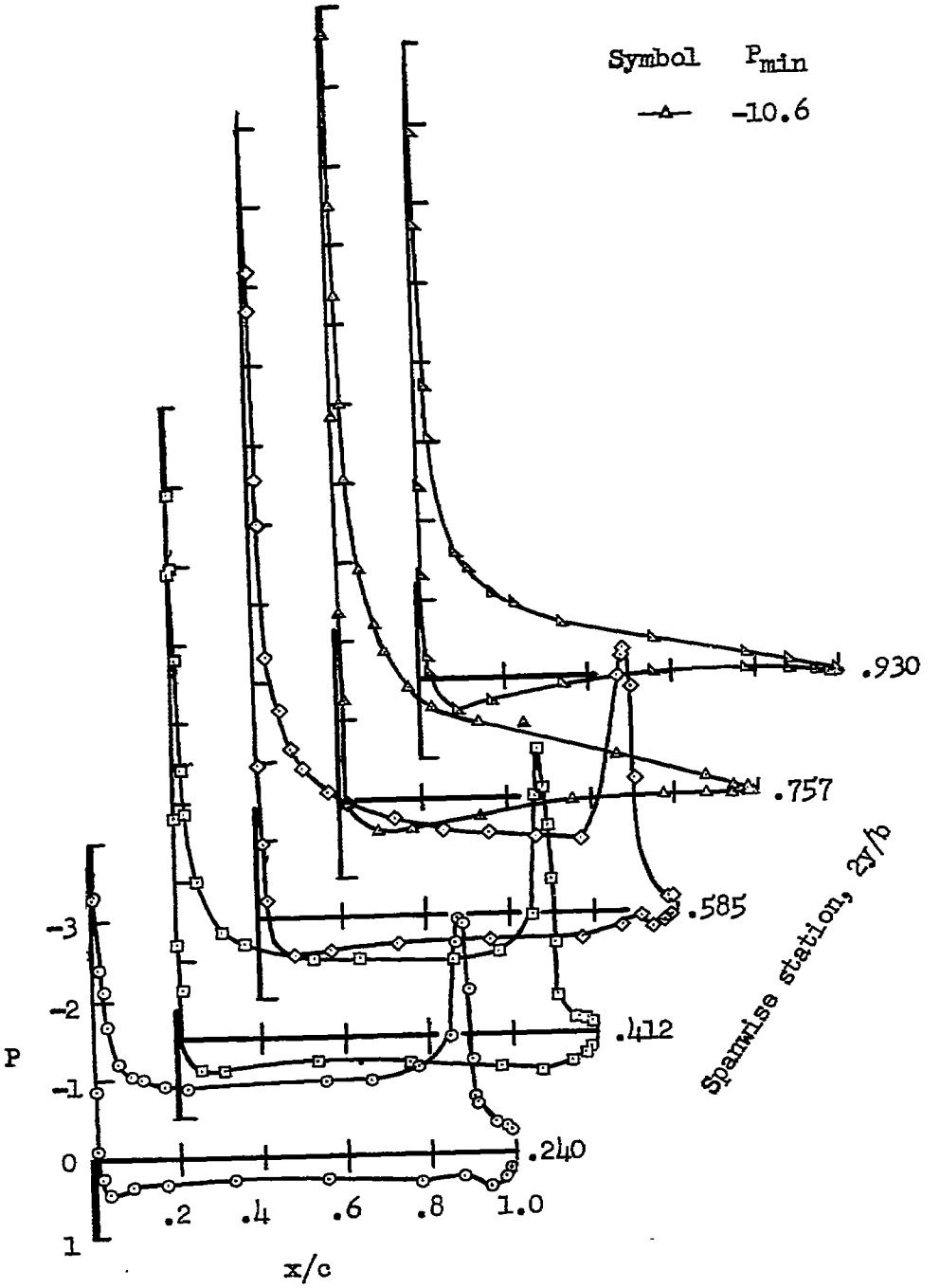

(b) $\alpha = 4.5^{\circ}$

Figure 15.- Continued

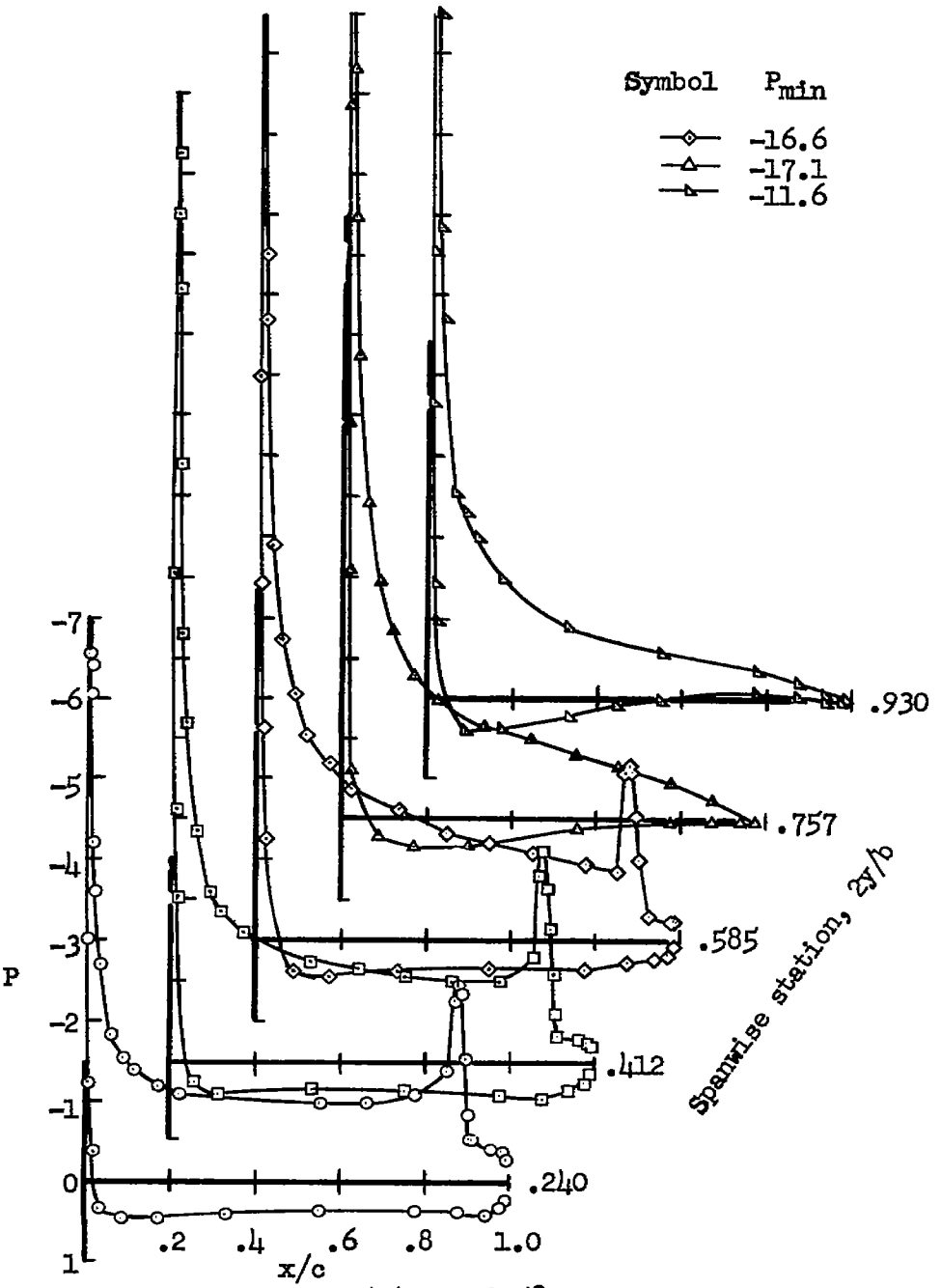

(c) $\alpha = 8.6^\circ$

Figure 15.- Continued.

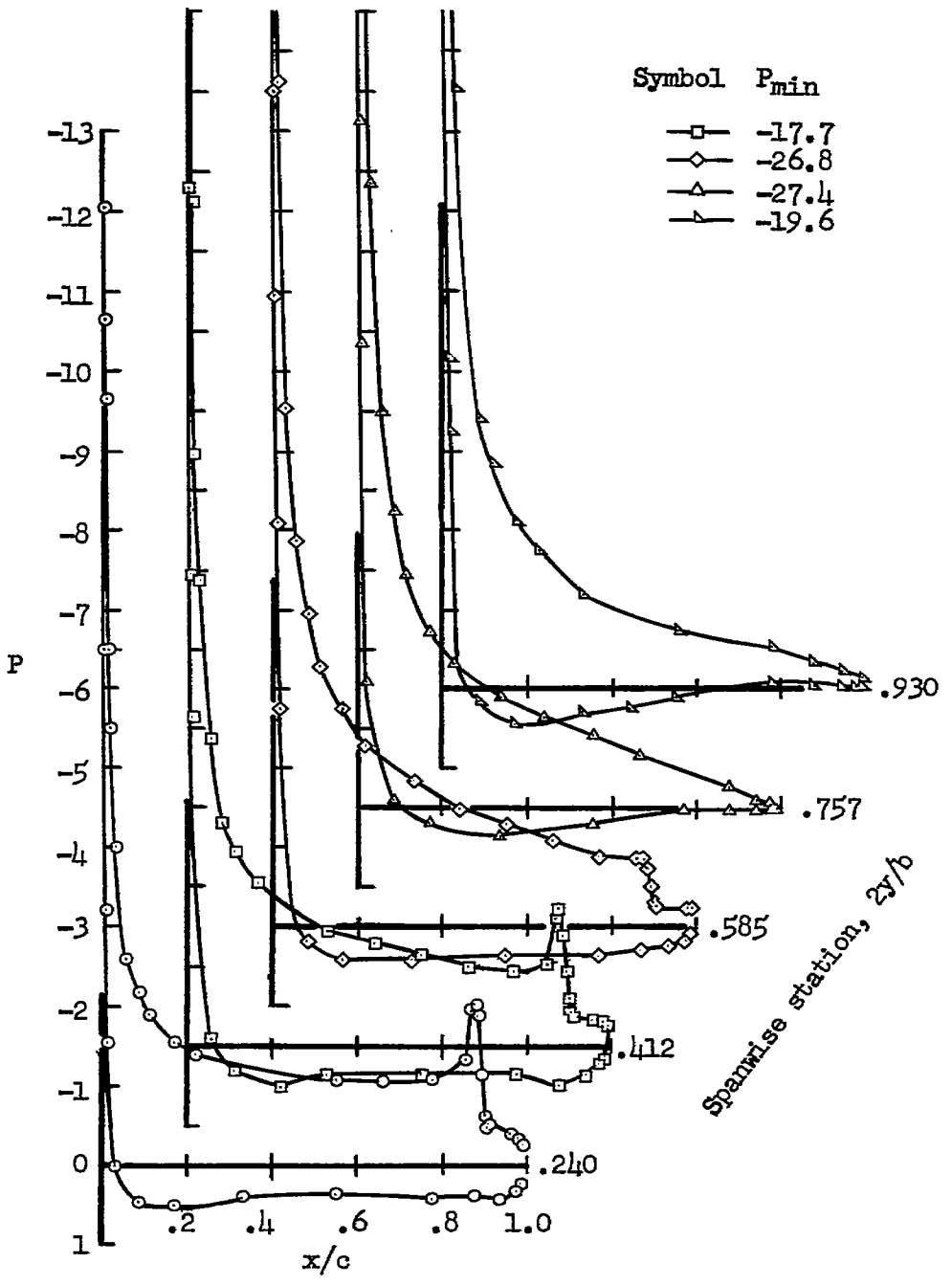

(d) $\alpha = 12.6^{\circ}$

Figure 15.- Continued.

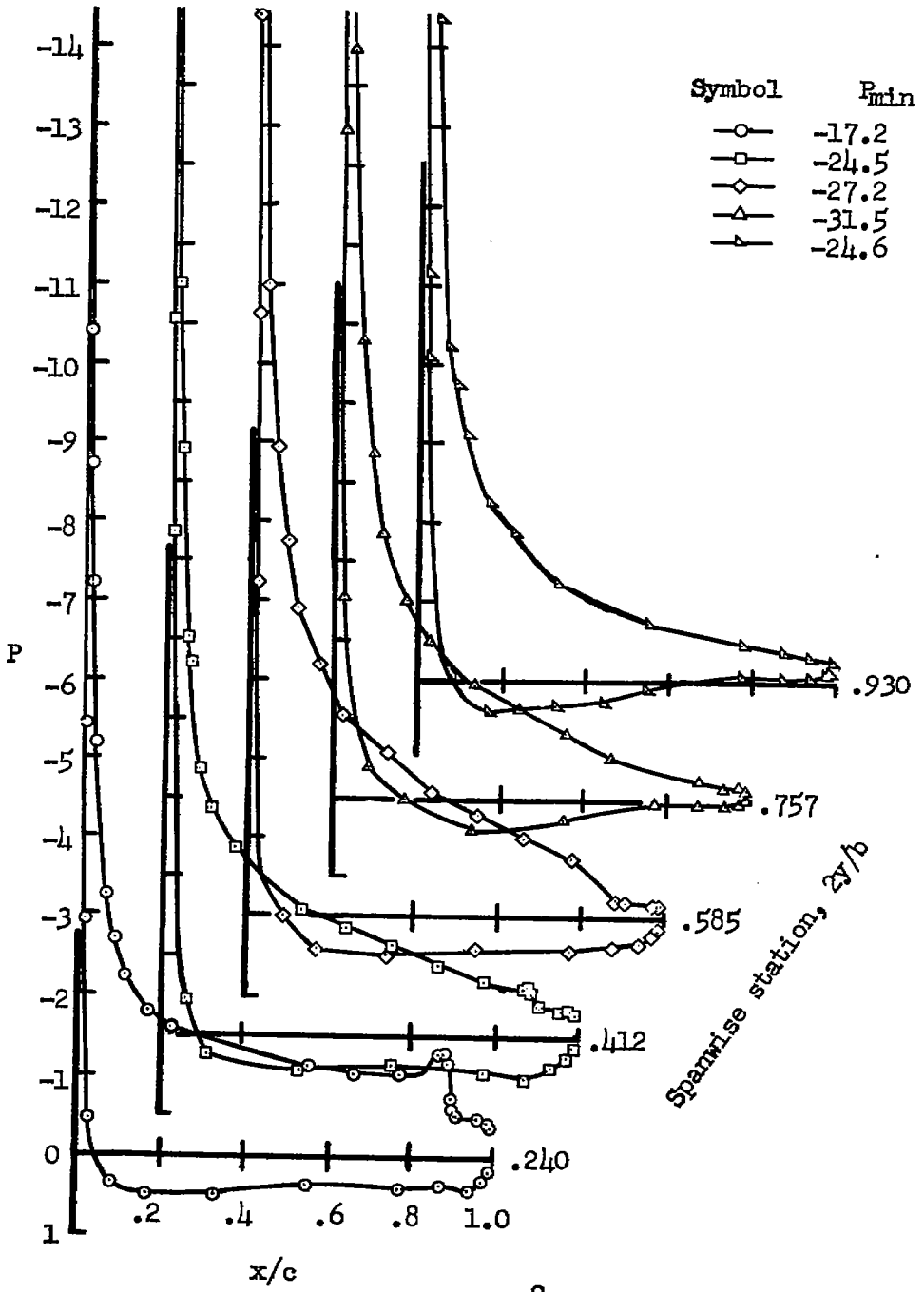

(e) $\alpha = 16.7^{\circ}$

Figure 15.- Concluded.

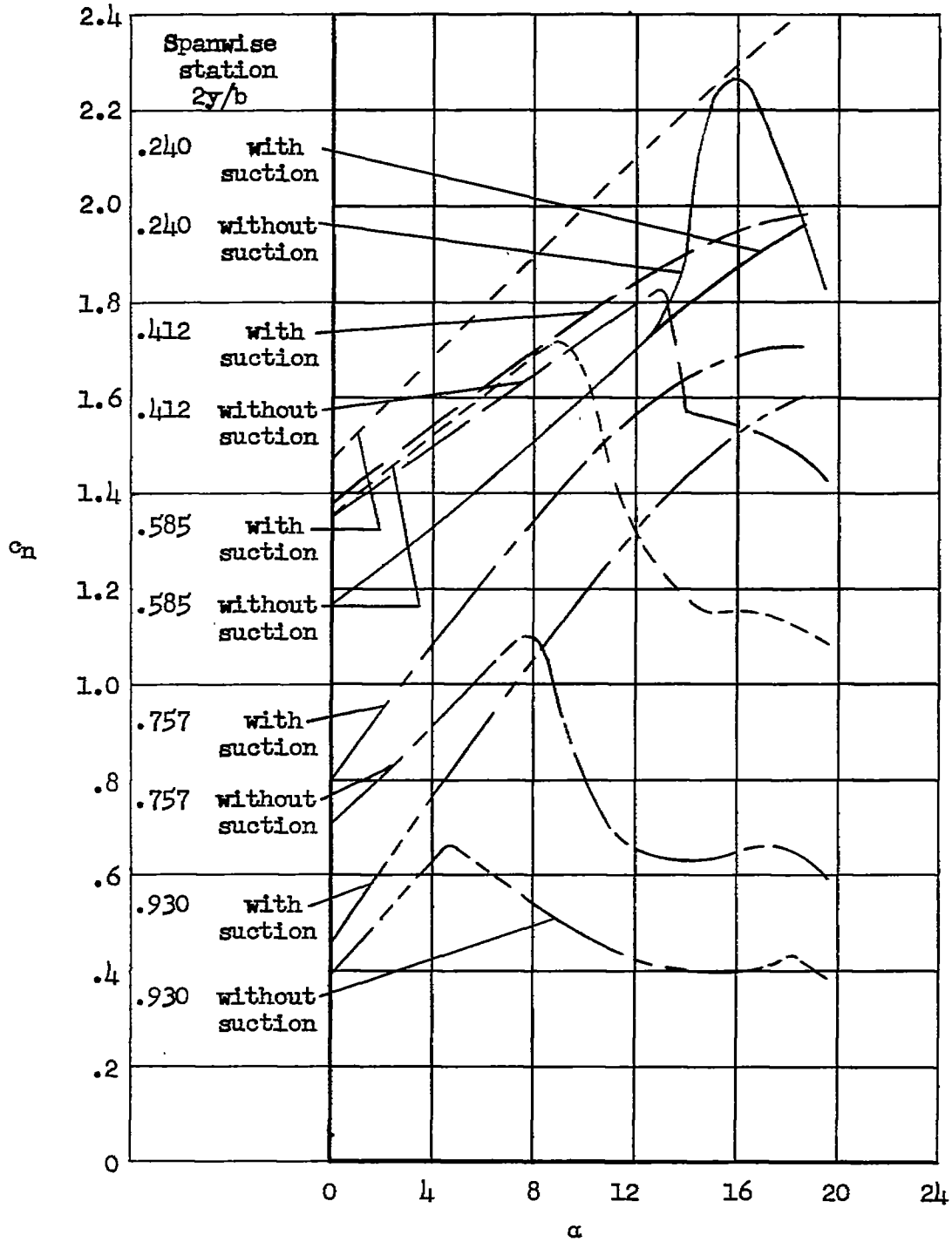

Figure 16.- Effect of area suction at the wing leading edge on the section normal-force coefficient curves for five spanwise stations on the wing with suction on the deflected flap; $\delta_f = 60^\circ$, flap span from 0.12 to 0.66 b/2.

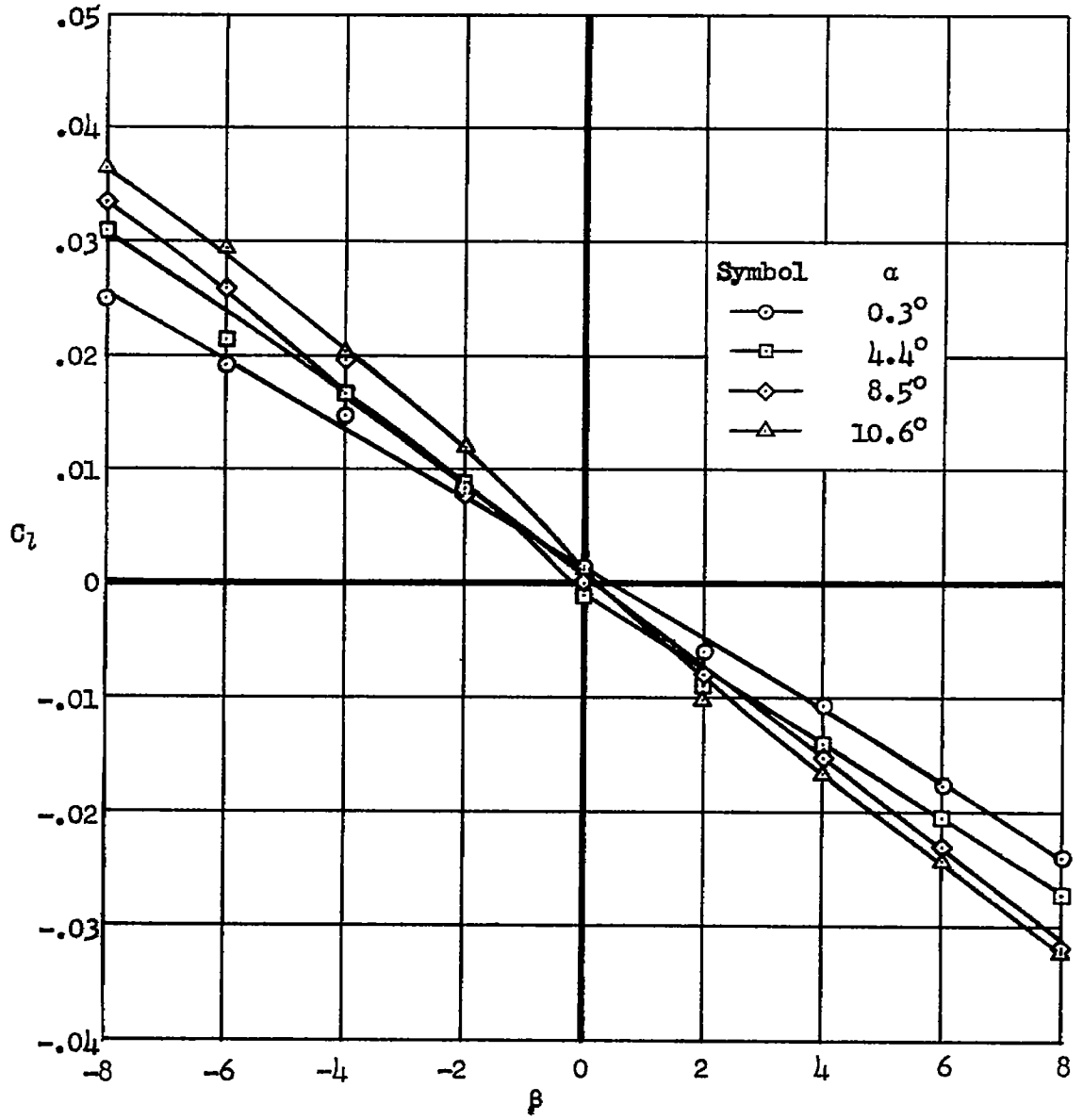

Figure 17.- Variation of rolling-moment coefficient with sideslip angle at various angles of attack with flaps deflected 55° from 0.12 to 0.50 b/2; boundary-layer control applied to flaps and wing leading edge.

[redacted]

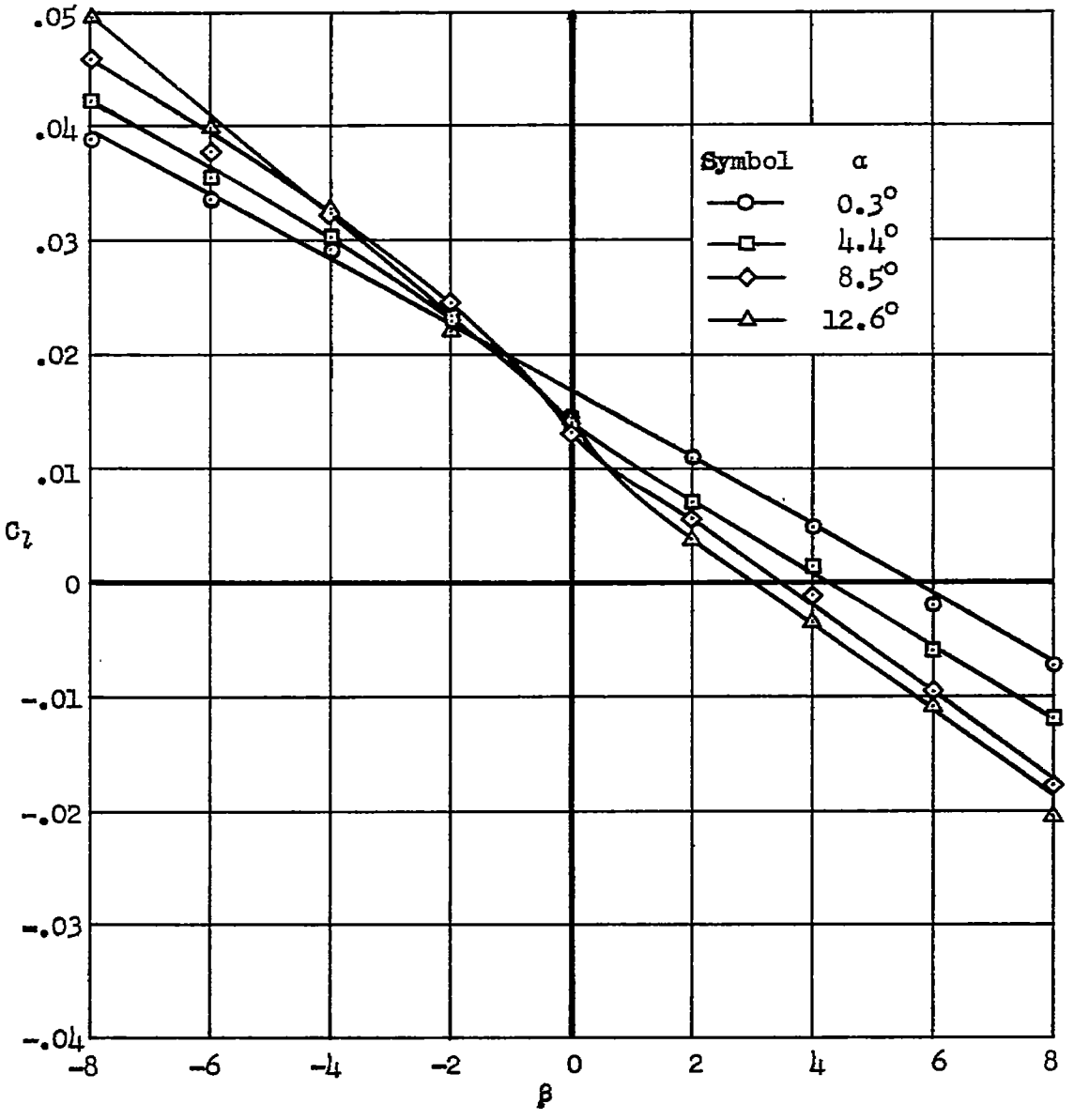

Figure 18.- Variation of rolling-moment coefficient with sideslip angle of the model at various angles of attack; left flaperon deflected 65° and right flaperon deflected 46°; boundary-layer control applied to flaperons and leading edge; flaperon span from 0.12 to 0.50 b/2.

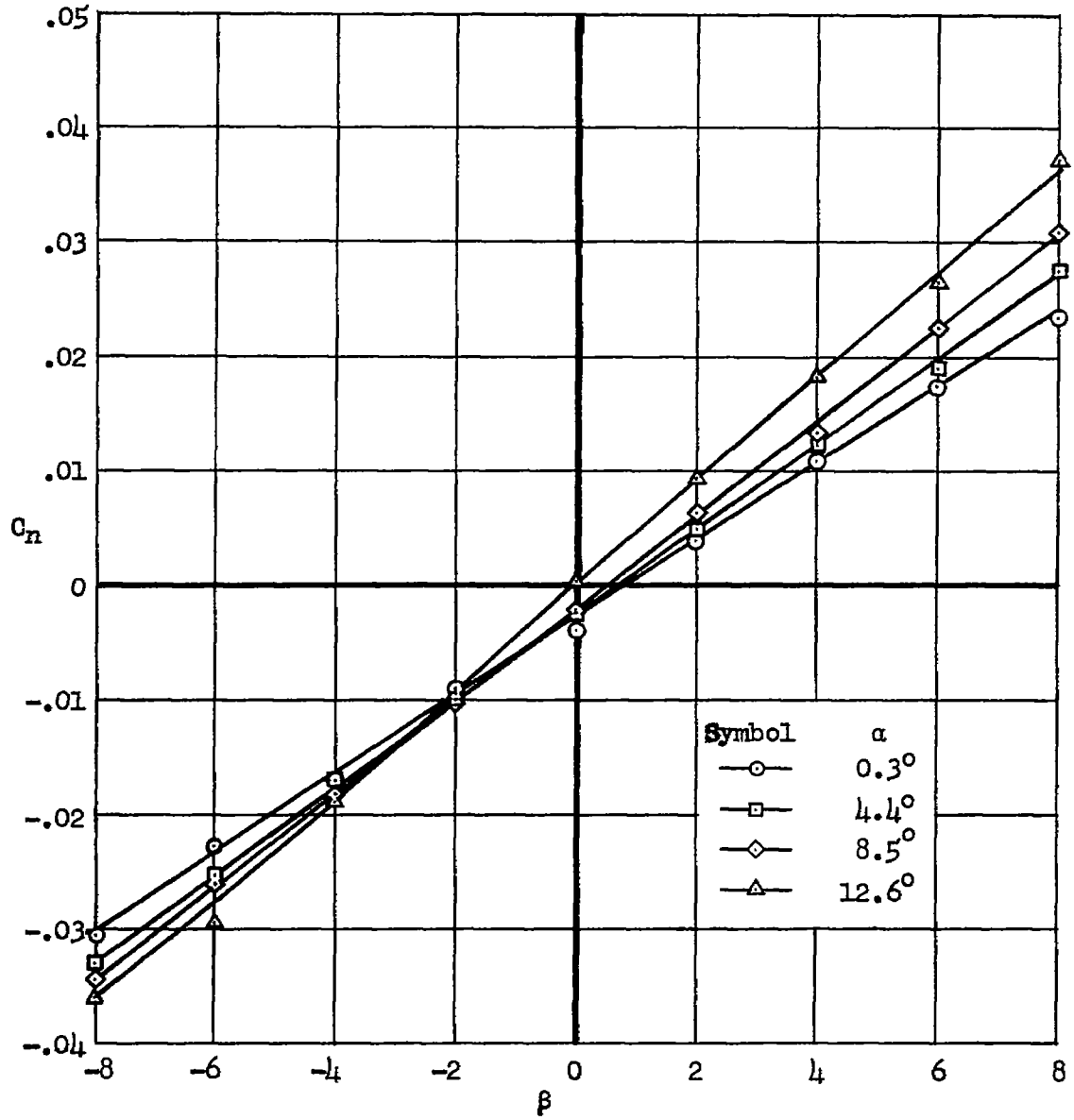

Figure 19.- Yawing-moment coefficient variation with sideslip angle of the model at various angles of attack; left flaperon deflected 65° and right flaperon deflected 46°; boundary-layer control applied to flaperons and leading edge; flaperon span from 0.12 to 0.50 b/2.

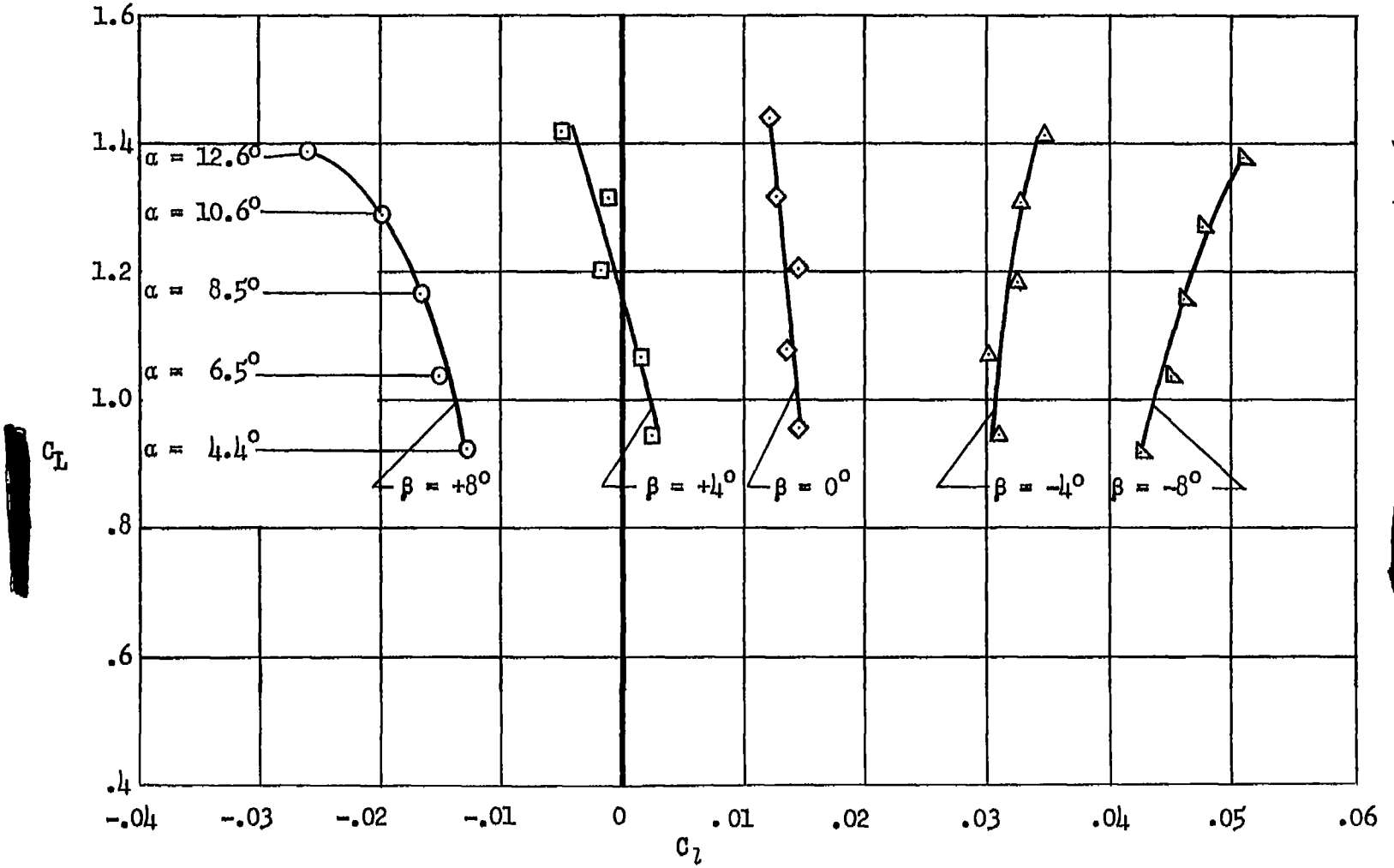

Figure 20.- Variation of rolling-moment coefficient with lift coefficient of the model at various sideslip angles; left flaperon deflected 65° and right flaperon deflected 46°, boundary-layer control applied to the flaperons and leading edge, flaperon span from 0.12 to 0.50 b/2.

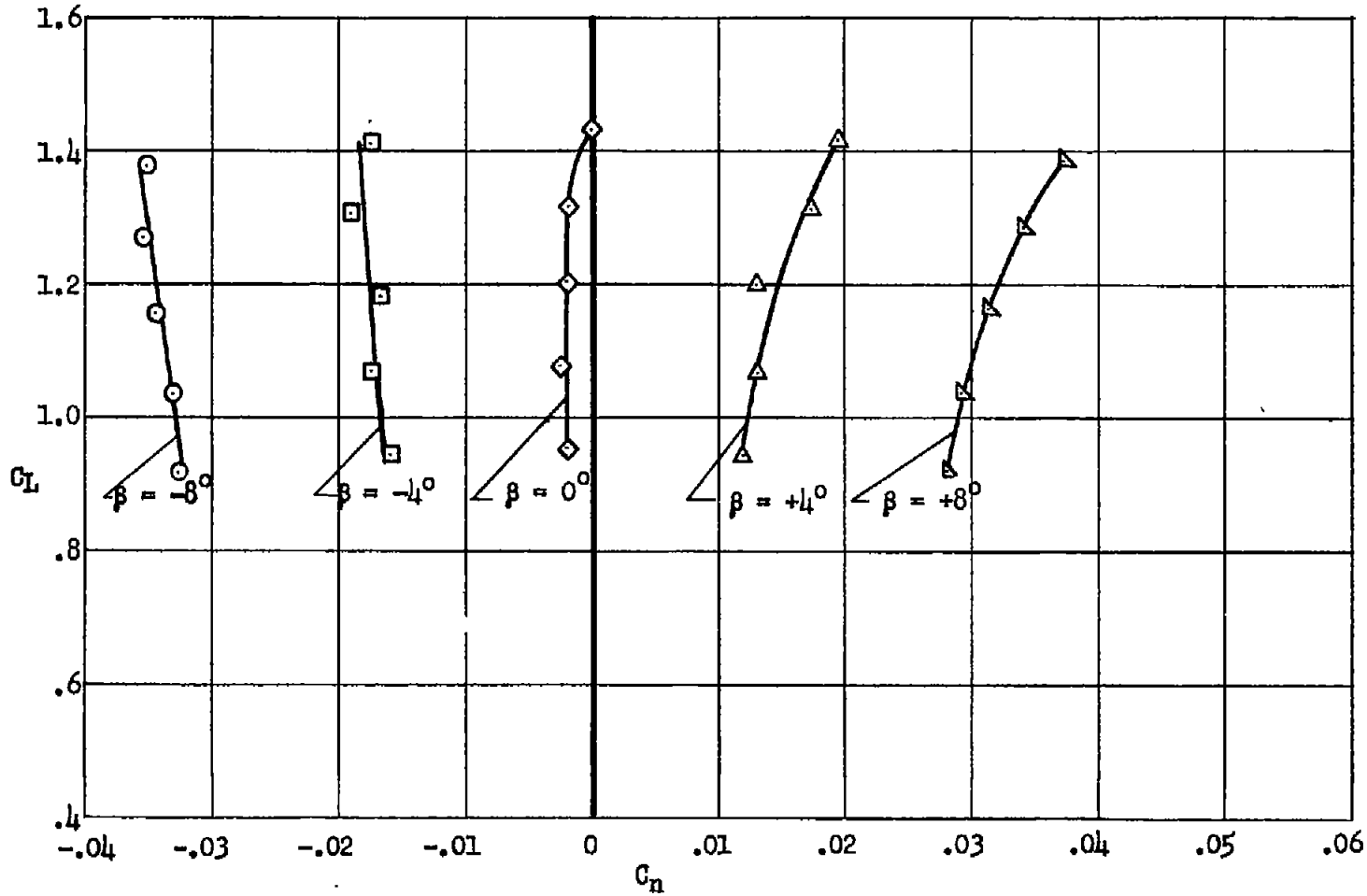

Figure 21.- Variation of yawing-moment coefficient with lift coefficient of the model at various sideslip angles; left flaperon deflected 65° and right flaperon deflected 46° with suction on flaperons and leading edge, flaperon span from 0.12 to 0.50 b/2.